IEC/IEEE 62704-1

Edition 1.0 2017-10

INTERNATIONAL STANDARD

Determining the peak spatial-average specific absorption rate (SAR) in the human body from wireless communications devices, 30 MHz to 6 GHz – Part 1: General requirements for using the finite-difference time-domain (FDTD) method for SAR calculations

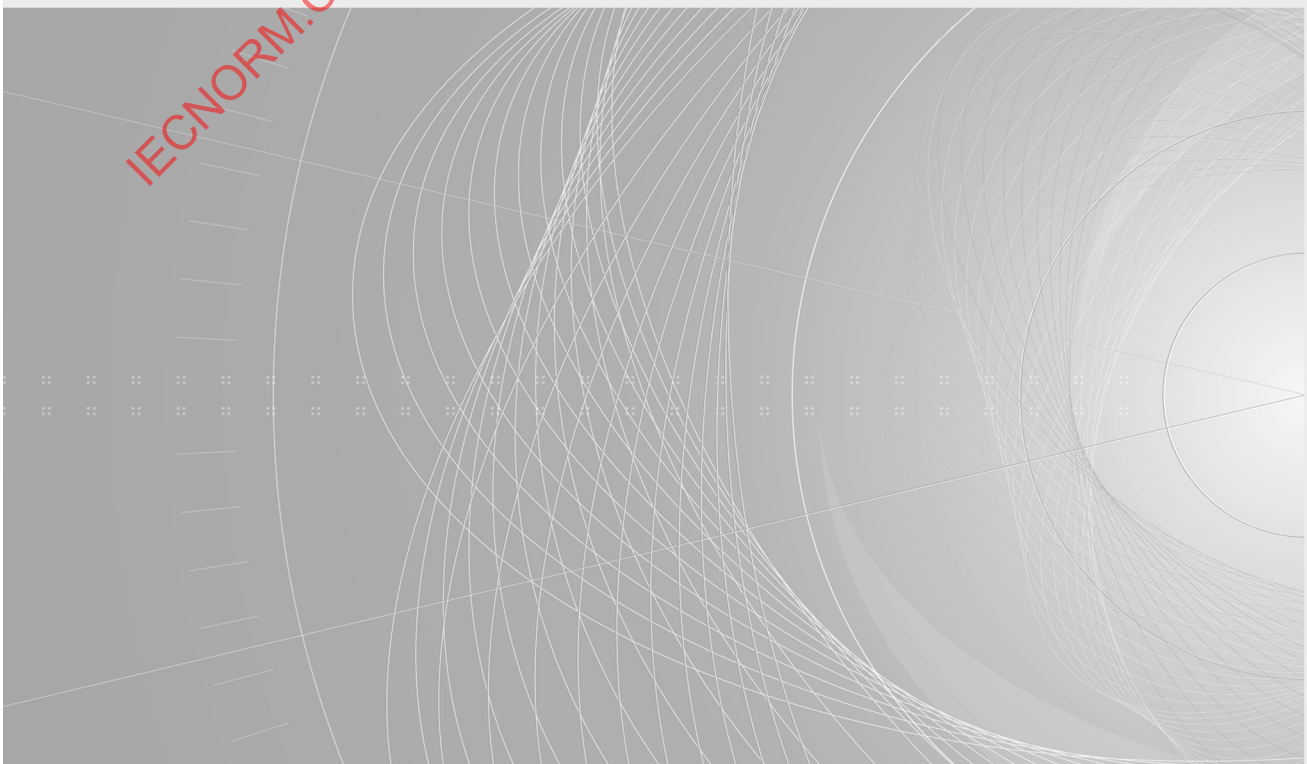

IEC/IEEE 62704-1:2017-10(en)

IEC Central Office
3, rue de Varembé
CH-1211 Geneva 20
Switzerland
Tel.: +41 22 919 02 11
Fax: +41 22 919 03 00
info@iec.ch
www.iec.ch

Institute of Electrical and Electronics Engineers, Inc.
3 Park Avenue
New York, NY 10016-5997
United States of America
stds.ipr@ieee.org
www.ieee.org

About the IEC
The International Electrotechnical Commission (IEC) is the leading global organization that prepares and publishes International Standards for all electrical, electronic and related technologies.

About the IEEE
IEEE is the world's largest professional association dedicated to advancing technological innovation and excellence for the benefit of humanity. IEEE and its members inspire a global community through its highly cited publications, conferences, technology standards, and professional and educational activities.

About IEC/IEEE publications
The technical content of IEC/IEEE publications is kept under constant review by the IEC and IEEE. Please make sure that you have the latest edition, a corrigendum or an amendment might have been published.

IEC Catalogue - webstore.iec.ch/catalogue
The stand-alone application for consulting the entire bibliographical information on IEC International Standards, Technical Specifications, Technical Reports and other documents. Available for PC, Mac OS, Android Tablets and iPad.

IEC publications search - www.iec.ch/searchpub
The advanced search enables to find IEC publications by a variety of criteria (reference number, text, technical committee,…). It also gives information on projects, replaced and withdrawn publications.

IEC Just Published - webstore.iec.ch/justpublished
Stay up to date on all new IEC publications. Just Published details all new publications released. Available online and also once a month by email.

Electropedia - www.electropedia.org
The world's leading online dictionary of electronic and electrical terms containing 20 000 terms and definitions in English and French, with equivalent terms in 16 additional languages. Also known as the International Electrotechnical Vocabulary (IEV) online.

IEC Glossary - std.iec.ch/glossary
65 000 electrotechnical terminology entries in English and French extracted from the Terms and Definitions clause of IEC publications issued since 2002. Some entries have been collected from earlier publications of IEC TC 37, 77, 86 and CISPR.

IEC Customer Service Centre - webstore.iec.ch/csc
If you wish to give us your feedback on this publication or need further assistance, please contact the Customer Service Centre: csc@iec.ch.

IEC/IEEE 62704-1

Edition 1.0 2017-10

INTERNATIONAL STANDARD

Determining the peak spatial-average specific absorption rate (SAR) in the human body from wireless communications devices, 30 MHz to 6 GHz – Part 1: General requirements for using the finite-difference time-domain (FDTD) method for SAR calculations

INTERNATIONAL
ELECTROTECHNICAL
COMMISSION

ICS 17.220.20; 33.060.20

ISBN 978-2-8322-4769-3

CONTENTS

INTERNATIONAL ELECTROTECHNICAL COMMISSION

_____

DETERMINING THE PEAK SPATIAL-AVERAGE SPECIFIC ABSORPTION RATE (SAR) IN THE HUMAN BODY FROM WIRELESS COMMUNICATIONS DEVICES, 30 MHz TO 6 GHz –

Part 1: General requirements for using the finite-difference time-domain (FDTD) method for SAR calculations

FOREWORD

1) The International Electrotechnical Commission (IEC) is a worldwide organization for standardization comprising all national electrotechnical committees (IEC National Committees). The object of IEC is to promote international co-operation on all questions concerning standardization in the electrical and electronic fields. To this end and in addition to other activities, IEC publishes International Standards, Technical Specifications, Technical Reports, Publicly Available Specifications (PAS) and Guides (hereafter referred to as "IEC Publication(s)"). Their preparation is entrusted to technical committees; any IEC National Committee interested in the subject dealt with may participate in this preparatory work. International, governmental and non-governmental organizations liaising with the IEC also participate in this preparation.

   IEEE Standards documents are developed within IEEE Societies and Standards Coordinating Committees of the IEEE Standards Association (IEEE-SA) Standards Board. IEEE develops its standards through a consensus development process, approved by the American National Standards Institute, which brings together volunteers representing varied viewpoints and interests to achieve the final product. Volunteers are not necessarily members of IEEE and serve without compensation. While IEEE administers the process and establishes rules to promote fairness in the consensus development process, IEEE does not independently evaluate, test, or verify the accuracy of any of the information contained in its standards. Use of IEEE Standards documents is wholly voluntary. *IEEE documents are made available for use subject to important notices and legal disclaimers (see* http://standards.ieee.org/IPR/disclaimers.html *for more information).*

   IEC collaborates closely with IEEE in accordance with conditions determined by agreement between the two organizations. This Dual Logo International Standard was jointly developed by the IEC and IEEE under the terms of that agreement.

2) The formal decisions of IEC on technical matters express, as nearly as possible, an international consensus of opinion on the relevant subjects since each technical committee has representation from all interested IEC National Committees. The formal decisions of IEEE on technical matters, once consensus within IEEE Societies and Standards Coordinating Committees has been reached, is determined by a balanced ballot of materially interested parties who indicate interest in reviewing the proposed standard. Final approval of the IEEE standards document is given by the IEEE Standards Association (IEEE-SA) Standards Board.

3) IEC/IEEE Publications have the form of recommendations for international use and are accepted by IEC National Committees/IEEE Societies in that sense. While all reasonable efforts are made to ensure that the technical content of IEC/IEEE Publications is accurate, IEC or IEEE cannot be held responsible for the way in which they are used or for any misinterpretation by any end user.

4) In order to promote international uniformity, IEC National Committees undertake to apply IEC Publications (including IEC/IEEE Publications) transparently to the maximum extent possible in their national and regional publications. Any divergence between any IEC/IEEE Publication and the corresponding national or regional publication shall be clearly indicated in the latter.

5) IEC and IEEE do not provide any attestation of conformity. Independent certification bodies provide conformity assessment services and, in some areas, access to IEC marks of conformity. IEC and IEEE are not responsible for any services carried out by independent certification bodies.

6) All users should ensure that they have the latest edition of this publication.

7) No liability shall attach to IEC or IEEE or their directors, employees, servants or agents including individual experts and members of technical committees and IEC National Committees, or volunteers of IEEE Societies and the Standards Coordinating Committees of the IEEE Standards Association (IEEE-SA) Standards Board, for any personal injury, property damage or other damage of any nature whatsoever, whether direct or indirect, or for costs (including legal fees) and expenses arising out of the publication, use of, or reliance upon, this IEC/IEEE Publication or any other IEC or IEEE Publications.

8) Attention is drawn to the normative references cited in this publication. Use of the referenced publications is indispensable for the correct application of this publication.

9) Attention is drawn to the possibility that implementation of this IEC/IEEE Publication may require use of material covered by patent rights. By publication of this standard, no position is taken with respect to the existence or validity of any patent rights in connection therewith. IEC or IEEE shall not be held responsible for identifying Essential Patent Claims for which a license may be required, for conducting inquiries into the legal validity or scope of Patent Claims or determining whether any licensing terms or conditions provided in connection with submission of a Letter of Assurance, if any, or in any licensing agreements are reasonable or non-discriminatory. Users of this standard are expressly advised that determination of the validity of any patent rights, and the risk of infringement of such rights, is entirely their own responsibility.

International Standard IEEE/IEC 62704-1 has been prepared by IEC technical committee 106: Methods for the assessment of electric, magnetic and electromagnetic fields associated with human exposure, in cooperation with the International Committee on Electromagnetic Safety of the IEEE Standards Association[1], under the IEC/IEEE Dual Logo Agreement.

This publication is published as an IEC/IEEE Dual Logo standard.

This standard contains attached files in the form of CAD models and reference results described in Annexes B and D. These files are available at: http://www.iec.ch/dyn/www/f?p=103:227:0::::FSP_ORG_ID,FSP_LANG_ID:1303,25.

The text of this standard is based on the following IEC documents:

FDIS	Report on voting
106/401A/FDIS	106/413/RVD

Full information on the voting for the approval of this standard can be found in the report on voting indicated in the above table.

International Standards are drafted in accordance with the rules given in the ISO/IEC Directives, Part 2.

A list of all parts in the IEC/IEEE 62704 series, published under the general title *Determining the peak spatial-average specific absorption rate (SAR) in the human body from wireless communications devices, 30 MHz to 6 GHz*, can be found on the IEC website.

The IEC technical committee and IEEE technical committee have decided that the contents of this publication will remain unchanged until the stability date indicated on the IEC web site under "http://webstore.iec.ch" in the data related to the specific publication. At this date, the publication will be

- reconfirmed,
- withdrawn,
- replaced by a revised edition, or
- amended.

1 A list of IEEE participants can be found at the following URL: http://standards.ieee.org/downloads/62704/62704-1-2017/62704-1-2017_wg-participants.pdf.

INTRODUCTION

Computational techniques have reached a level of maturity which allows their use in specific absorption rate (SAR) assessment of wireless communication devices. Some wireless communication devices are used in situations where experimental SAR assessment is extremely complex or not possible at all. National regulatory bodies (e.g. US Federal Communications Commission) encourage the development of consensus standards and encouraged the establishment of the ICES Technical Committee 34 Subcommittee 2. The benefits to the users and the regulators include standardized and accepted protocols, anatomically correct body models, validation techniques, benchmark data, reporting format and means for estimating the computational uncertainty in order to produce valid, accurate, repeatable, and reproducible data.

DETERMINING THE PEAK SPATIAL-AVERAGE SPECIFIC ABSORPTION RATE (SAR) IN THE HUMAN BODY FROM WIRELESS COMMUNICATIONS DEVICES, 30 MHz TO 6 GHz –

Part 1: General requirements for using the finite-difference time-domain (FDTD) method for SAR calculations

1 Scope

This part of IEC/IEEE 62704 defines the methodology for the application of the finite-difference time domain (FDTD) technique when used for determining the peak spatial-average specific absorption rate (SAR) in the human body exposed to wireless communication devices with known uncertainty. It defines methods to validate the numerical model of the device under test (DUT) and to assess its uncertainty when used in SAR simulations. Moreover, it defines procedures to determine the peak spatial-average SAR in a cubical volume and to validate the correct implementation of the FDTD simulation software. The applicable frequency range is 30 MHz to 6 GHz.

NOTE Cubical averaging volumes are applied in all current experimental standards for the assessment of the peak spatial-average SAR (psSAR) and recommended by [1], [2] and [3]. Other averaging volumes have been proposed, for example, in [1], and may be included in future revisions of this document.

This document does not recommend specific SAR limits since these are found elsewhere, for example, in the guidelines published by the International Commission on Non-Ionizing Radiation Protection (ICNIRP) [1] or in IEEE Std C95.1 [3].

2 Normative references

The following documents are referred to in the text in such a way that some or all of their content constitutes requirements of this document. For dated references, only the edition cited applies. For undated references, the latest edition of the referenced document (including any amendments) applies.

NOTE The experimental standards that define the SAM phantom and the testing positions are IEEE Std 1528 and IEC 62209-1.

IEEE Std 1528, *IEEE Recommended Practice for Determining the Peak Spatial-Average Specific Absorption Rate (SAR) in the Human Head from Wireless Communications Devices: Measurement Techniques*

IEC 62209-1, *Human Exposure to Radio Frequency Fields from Hand Held and Body Mounted Wireless Communication Devices – Human Models, Instrumentation and Procedures – Part 1: Procedure to determine the specific absorption rate (SAR) for devices used next to the ear (frequency range of 300 MHz to 6 GHz)*

IEC 60050 (all parts), *International Electrotechnical Vocabulary (IEV)* (available at: http://www.electropedia.org)

IEEE Standards Dictionary Online (subscription available at: http://dictionary.ieee.org)

3 Terms and definitions

For the purposes of this document, the terms and definitions given in the IEEE Standards Dictionary Online, IEC 60050 (all parts) and the following apply.

ISO, IEC and IEEE maintain terminological databases for use in standardization at the following addresses:

- IEC Electropedia: available at http://www.electropedia.org/
- ISO Online browsing platform: available at http://www.iso.org/obp
- IEEE Dictionary Online: available at http://dictionary.ieee.org

3.1
excitation source
source with an associated signal which feeds electric or magnetic energy to one or more edges of the mesh

Note 1 to entry: The amplitude of the signal is proportional to an arbitrary function of time.

3.1.1
added source
source whose amplitude is added to the present value of an E-field component on a mesh edge at each time step of the FDTD algorithm

3.1.2
hard source
source whose amplitude replaces the present value of an E-field component on a mesh edge at each time step of the FDTD algorithm

3.1.3
voltage source
source whose amplitude updates the present value of an E-field component on a mesh edge at each time step of the FDTD algorithm considering the current through the mesh edge represented by its surrounding H-fields and an internal resistance

3.2
antenna
part of a transmitting or receiving system that is designed to radiate or to receive electromagnetic waves

3.3
feed-point
<antenna> part of the radiating structure where the radio-frequency currents start to support the electromagnetic fields that carry energy away from the antenna

Note 1 to entry: Often the feed-point of the antenna is not accessible because of mechanical support requirements; in this case a connection point is available to inject radio-frequency energy into the antenna. Normally, the connection point is a simple connector or a waveguide flange. If not collocated, the connection and the feed-point of an antenna are interconnected by one or more sections of transmission line. By measuring the antenna impedance at the connection point, if the electrical characteristics of the transmission lines between the connection and the feed-point are known, it is possible to calculate the driving point or feed-point impedance of an antenna.

3.4
antenna feed-point impedance
terminal or driving-point impedance
ratio of complex voltage to complex current at the terminals of a transmitting antenna, or the ratio of the open-circuit voltage to the short-circuit current at the terminals of a receiving antenna

3.5
attenuation
decrease in magnitude of a field quantity in the transmission from one point to another

Note 1 to entry: Attenuation is expressed as a ratio.

3.6
average power
$\overline{P}$
time-averaged rate of energy transfer

$$\overline{P} = \frac{1}{t_2 - t_1} \int_{t_1}^{t_2} P(t)\,\mathrm{d}t \quad (1)$$

where $P(t)$ is the instantaneous power

Note 1 to entry: The time duration could be source related (for example, the source repetition period, duty cycle) or use related.

3.7
background material
material or tissue which is not considered for the averaging volume

Note 1 to entry: Most typically, a background material will be any lossless material, such as the free-space or air surrounding the anatomical model. It also includes air enclosures or other lumina inside the body and tissues that have been excluded from averaging, for example, by user selection.

3.8
benchmark simulation
simulation test specifically defined to validate simulation results based on comparison with a reference

3.9
body
geometrical distribution of the dielectric properties and the mass densities of all live body tissues including body fluids

Note 1 to entry: The contents of body lumina or foreign matter, such as medical implants or jewellery, are not considered as part of the body.

3.10
conductivity
σ
ratio of the magnitude of the conduction-current density in a medium to the electric field strength

Note 1 to entry: Conductivity is expressed in units of siemens per metre (S/m).

3.11
conservative estimate
estimate of the peak spatial-average SAR and whole-body average SAR as defined in this document that is representative of what is expected to occur in the body of a significant majority of population during normal operating conditions of wireless communication devices

Note 1 to entry: Conservative estimate does not mean the absolute maximum SAR value that could possibly occur under every conceivable combination in the human body size, shape separation from the antenna and/or vehicle.

3.12
coverage factor
k
factor that is used to obtain the expanded uncertainty from the combined uncertainty with a known probability (P) of containing the true value of the measurand

Note 1 to entry: Specifically, k × (combined uncertainty) = (expanded uncertainty). When $k = 1$, $P \approx 0{,}68$; $k = 2$, $P \approx 0{,}95$; $k = 3$, $P \sim 0{,}999$.

3.13
electric field
E-field
vector field of electric field strength

3.14
electric field strength
E
at a given point, the magnitude (modulus) of the vector limit of the quotient of the force that a small stationary charge at that point will experience, by virtue of its charge, to the charge as the charge approaches zero in a macroscopic sense

Note 1 to entry: This may be measured either in newtons per coulomb or in volts per metre. This term is sometimes called the E-field intensity, but such use of the word intensity is deprecated, since intensity connotes power in optics and radiation.

3.14.1
electric field strength
<signal-transmission system> magnitude of the potential gradient in an E-field expressed in units of potential difference per unit length in the direction of the gradient

3.14.2
electric field strength
<radio wave propagation> magnitude of the E-field vector

Note 1 to entry: The electric field strength is expressed in volts per metre (V/m)

3.15
electrical length
length of a transmission medium or a transmission line, such as an antenna or a waveguide in any medium including air

Note 1 to entry: Electrical length is expressed in wavelengths, radians, or degrees. When expressed in angular units, it is a distance in wavelengths multiplied by 2π to yield radians, or by 360 to yield degrees.

3.16
electromagnetic field
EM field
electromagnetic phenomenon expressed in scalar or vector functions of space and time, for example, a time-varying field associated with electric and magnetic forces and described by Maxwell's equations

3.17
far-field region
region of the field of an antenna where the angular field distribution is essentially, independent of the distance from the antenna

Note 1 to entry: In this region (also called the free-space region), the field has predominantly plane wave characteristics, i.e. the electric field strength and magnetic field strength distributions are locally uniform in planes transverse to the direction of propagation.

Note 2 to entry: For larger antennas especially, the far-field region is also referred to as the Fraunhofer region.

3.18
incident wave
wave, travelling through a medium, in a specific direction, which impinges on a discontinuity or a medium of different propagation characteristics

3.19
magnetic field
H-field
vector field of magnetic field strength

3.20
magnetic field strength
H
magnitude of the magnetic field vector

Note 1 to entry: The magnetic field strength is expressed in amperes per metre (A/m).

Note 2 to entry: For time harmonic fields in a medium with linear and isotropic magnetic properties, H is equal to the ratio of the magnetic flux density B to the magnetic permeability of the medium μ, i.e., $H = B/\mu$.

3.21
mesh
discrete representation of the simulation model as a set of voxels in a regular three-dimensional Cartesian arrangement

Note 1 to entry: In the scientific literature, the mesh is often referred to as “grid”.

3.22
near-field region
region in the field of an antenna, located near the antenna, in which the electric and magnetic fields do not have substantial plane-wave characteristics, but vary considerably from point to point

Note 1 to entry: The term near-field region is often vaguely defined and has different meanings for large and small antennas. The near-field region is further subdivided into the reactive near-field region, which is closest to the antenna and contains most or nearly all of the stored energy associated with the field of the antenna, and the radiating near-field region. If the antenna has a maximum overall dimension that is not large compared to the wavelength, the radiating near-field region may not exist. For antennas large in terms of wavelength, the radiating near-field region is sometimes referred to as the Fresnel region.

Note 2 to entry: For most antennas, the outer boundary of the reactive near-field region is commonly taken to exist at a distance of $\lambda/2\pi$ from the antenna surface.

3.23
perfect electric conductor
PEC
material with infinite electrical conductivity which does not dissipate any energy

3.24
relative permittivity
ε_r
ratio of the complex permittivity to the permittivity of free space

Note 1 to entry: The complex relative permittivity, $\varepsilon_r = \varepsilon/\varepsilon_o$, of an isotropic, linear, lossy dielectric medium is given by $\varepsilon_r = \varepsilon_r' - j\varepsilon_r'' = \varepsilon_r' - j\frac{\sigma}{\omega\varepsilon_0} = \varepsilon_r'\left(1 - j\frac{\varepsilon_r''}{\varepsilon_r'}\right) = \varepsilon_r'(1 - j\tan\delta)$

where

ε_0 is the free space permittivity (8,854 × 10^{-12} F/m);

ε_r' is the relative permittivity or dielectric constant;

σ is the conductivity in siemens per metre (S/m);

$\tan\delta$ is the loss tangent.

Note 2 to entry: For purposes of this document, the convention $e^{j\omega t}$ is used to describe time-varying electric fields.

Note 3 to entry: The permittivity of biological tissues is frequency dependent and may be a complex tensor quantity.

3.25
penetration depth
for a given frequency, the depth at which the electric field (E-field) strength of an incident plane wave, penetrating into a lossy medium, is reduced to $1/e$ of its value just beneath the surface of the lossy medium

Note 1 to entry: For a plane-wave incident normally on a planar half-space, the penetration depth δ is given in Formula (2):

$$\delta = \frac{1}{\omega}\left[\frac{\mu_0\varepsilon'_r\varepsilon_0}{2}\left(\sqrt{1+\left(\frac{\sigma}{\omega\varepsilon'_r\varepsilon_0}\right)^2}-1\right)\right]^{-1/2} \quad (2)$$

3.26
permeability
μ
ratio of the magnetic flux density to the magnetic field strength at a point

Note 1 to entry: The permeability is expressed in units of henry per metre (H/m).

3.27
reactive field
electric and magnetic fields surrounding an antenna or other electromagnetic devices that result in storage rather than propagation of electromagnetic energy

3.28
root-mean-square value
rms
<of a periodic function> positive square root of the mean value of the square of the function taken over a given period

Note 1 to entry: For a periodic function y of t, the positive square root of y is

$$Y_{\text{rms}} = \left[\frac{1}{T}\int y(t)^2\,dt\right]^{1/2} \quad (3)$$

where

Y_{rms} is the rms value of y;
t is any value of time;
T is the period.

3.29
root-sum-square value
rss
positive square root of the sum of the squares of the elements of a set of numbers

3.30
scattering
process that causes waves incident on discontinuities or boundaries of media to be changed in direction, phase, or polarization

3.31
specific absorption rate
SAR
time derivative (rate) of the incremental energy (dW) absorbed by (dissipated in) an incremental mass (dm) contained in a volume element (dV) of a given density (ρ):

$$SAR = \frac{\mathrm{d}}{\mathrm{d}t}\left(\frac{\mathrm{d}W}{\mathrm{d}m}\right) = \frac{\mathrm{d}}{\mathrm{d}t}\left(\frac{\mathrm{d}W}{\rho\,\mathrm{d}V}\right) \quad (4)$$

Note 1 to entry: SAR is expressed in units of watts per kilogram (W/kg) or equivalently milliwatts per gram (mW/g).

Note 2 to entry: SAR can be related to the E-field at a point by

$$SAR = \frac{\sigma |\boldsymbol{E}|^2}{2\rho}$$

where

σ is the conductivity of the tissue in siemens per metre (S/m);

ρ is the mass density of the tissue in kilograms per cubic metre (kg/m^3);

$\boldsymbol{E}$ is the peak electric field vector in volts per metre (V/m).

Note 3 to entry: SAR can be related to the increase in temperature at a point by

$$SAR \approx \left.\frac{c\Delta T}{\Delta t}\right|_{t=0}$$

where

ΔT is the change in temperature in degree Celsius (ºC);

Δt is the duration of exposure in seconds (s);

c is the specific heat capacity in joules per kilogram and degree Celsius (J/kg ºC).

This assumes that measurements are made under “ideal” circumstances, i.e. no heat loss by thermal diffusion, heat radiation, or thermoregulation (blood flow, sweating, etc.). Moreover, this expression is valid only in the initial, linear regime of the temperature-time curve. If this linear regime does not exist, the provided expression is not used.

3.31.1
peak spatial-average specific absorption rate
maximum average SAR within a local region based on a specific averaging volume or mass

Note 1 to entry: SAR is expressed in watts per kilogram (W/kg) or equivalently milliwatts per gram (mW/g).

Note 2 to entry: The specific averaging volume or mass can be, for example, any 1 g or 10 g of tissue in the shape of a cube.

Note 3 to entry: For the purpose of this document, when the averaging mass is not specified the peak spatial-average SAR refers to both 1 g and 10 g quantities. In several tables in this document, the peak spatial-average SAR for 1 g and 10 g is simply denoted as 1 g and 10 g SAR.

3.31.2
spatial-average specific absorption rate
SAR within a local region based on a specific averaging volume or mass

Note 1 to entry: SAR is expressed in watts per kilogram (W/kg) or equivalently milliwatts per gram (mW/g).

Note 2 to entry: The specific averaging volume or mass can be, for example, any 1 g or 10 g of tissue in the shape of a cube.

3.32
whole body average specific absorption rate
quantity calculated as the power dissipated in the entire body divided by its mass

Note 1 to entry: SAR is expressed in watts per kilogram (W/kg) or equivalently milliwatts per gram (mW/g).

3.33
steady-state feed-point current
electric current flowing through the antenna feed-point in the steady-state regime of harmonic excitation at the operating frequency

3.34
steady-state feed-point voltage
voltage established at the antenna feed-point in the steady-state regime of harmonic excitation at the operating frequency

3.35
update coefficient
numerical value assigned to the voxel edges and faces calculated from the dielectric and magnetic properties of the voxels that surround it

Note 1 to entry: The update coefficient is used to advance the numerical values of the electric and magnetic fields in the mesh in time based on their present and past values.

3.36
voxel
volume element of the geometry to be discretized in the mesh

Note 1 to entry: In FDTD simulations for SAR calculation, the voxel is assigned the permittivity, permeability, the electric and magnetic conductivities and the mass density of the geometry. The E-field components of the mesh are located in a tangential direction on the centres of the voxel edges, and the H-field components of the mesh are located in a normal direction on the centres of the voxel faces. Each edge and face is assigned an update coefficient.

4 Abbreviated terms

ABC	Absorbing Boundary Condition
ASCII	American Standard Code for Information Interchange
CFL	Courant Friedrich Lewy
CT	Computed Tomography
DFT	Discrete Fourier Transformation
DUT	Device Under Test
FDTD	Finite-Difference Time-Domain
FFT	Fast Fourier Transformation
FIT	Finite Integration Technique
MIMO	Multiple Input Multiple Output
MRI	Magnetic Resonance Imaging
PEC	Perfect Electric Conductor
PMC	Perfect Magnetic Conductor
PML	Perfectly Matched layers
psSAR	Peak Spatial-Average Specific Absorption Rate
RMS	Root Mean Square
RSS	Root Sum Square
SAR	Specific Absorption Rate

5 Finite-difference time-domain method – basic definition

This document applies the finite-difference time-domain (FDTD) method to calculate SAR. FDTD is extensively used for bio-electromagnetic calculations, dating back to 1975 for the analysis of microwave heating of a human eye (Taflove and Brodwin [4]). In order to determine applicability of this document, it shall be clear whether a specific numerical solution of Maxwell's equations qualifies as an implementation of FDTD.

This is not entirely straightforward since there have been many variations of the FDTD method developed over the time since Kane Yee's original paper in 1966 [5], which may be taken as defining the fundamental FDTD method. Since then, the method has received significant attention in the scientific community. Numerous articles on the method and its extensions and applications have been published. Several text books on the FDTD method recapitulate its fundamentals, its further developments and its use ([6], [7], [8]). Details on the application of the FDTD method are given in Annex C.

This document is based in part on the extensive validation of FDTD as it applies to SAR calculation reported in the literature. Therefore, for the application of this document, the implementation of FDTD in the spatial region where SAR is being calculated shall include the following characteristics.

- The electric field components are spatially located on the edges of a Cartesian coordinate system structured mesh composed of rectangular parallelepipeds.
- The magnetic field components are spatially located on the edges of a Cartesian coordinate system structured mesh composed of rectangular parallelepipeds which is offset from the electric field mesh by a half-voxel in each direction.
- The numerical solution method is a finite-difference approximation of the Maxwell curl equations using central differences which are (at least globally) second-order accurate and would therefore include non-uniform meshes, which are also second-order accurate (Monk and Süli [9]).
- The numerical solution method solves for both electric and magnetic fields by a fully explicit leapfrog time-stepping process.
- Gauss's laws are implicitly enforced, the fields are divergence-free, and charge is conserved.
- The time-stepping algorithm is non-dissipative. Thus, there is no spurious decay of energy due to non-physical artefacts of the algorithm, and artificial dissipation is not required for stability.

NOTE Complex numerical dispersion in non-uniform meshes leads to spurious rise or decay of field amplitudes [9]. For the applications of the scope of this document, these effects are generally negligible. The impact of the numerical dispersion is assessed within the uncertainty evaluation (Clause 7).

Artificial dissipation may be introduced in certain finite-difference algorithms in order to prevent or limit the spurious generation of energy in the computational domain which can lead to numerical instabilities. Such artificial dispersion is not required for the FDTD algorithm as defined here.

The basic requirements on the FDTD method are given in Annex A. Other methods and/or extensions of FDTD that satisfy the above definitions but provide additional features may be applied provided that they have been fully validated according to the procedures in this document; code validation and benchmarks, etc. However, these alternative methods shall provide at least the same accuracy as the FDTD method defined above. The finite integration technique (FIT) in time domain can be regarded as an extension of FDTD in this context.

6 SAR calculation and averaging

6.1 Calculation of SAR in FDTD voxels

Since the electric fields in the FDTD mesh are located on the voxel edges, the x-, y-, and z-directed power components associated with a voxel are defined in different spatial locations. For SAR calculations, these components shall be summed with a defined mathematical procedure (see below).

The 12-field-components approach correctly interpolates all components in the centre of the voxel (using linear interpolation), defining the power dissipation at the voxel centre for which tissue density and conductivity can be unambiguously specified (D.1). Since all the field components used in the interpolation are tangential components of the voxel faces, the constitutive relations hold even if the voxel is located at interfaces of different materials or tissue types. The numerical accuracy of the interpolation with respect to the SAR calculation is discussed in [11]. This approach does not compromise the accuracy of the computed results since the order of accuracy of the interpolations involved is the same as that of the underlying FDTD data.

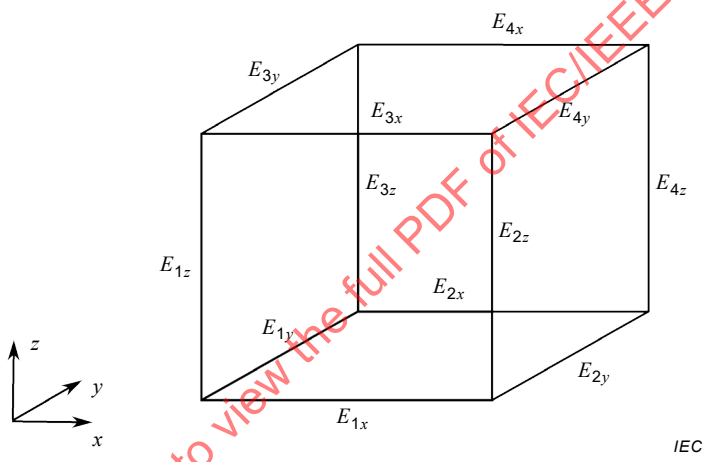

Figure 1 – Field components on voxel edges

To compute the SAR for a single FDTD voxel using the 12-field-components approach, the complex vector components of the complex amplitude of the E-field at each individual voxel edge shall be averaged into the voxel centre using linear interpolation:

$$E_x = \frac{1}{4}\left(E_{1x} + E_{2x} + E_{3x} + E_{4x}\right) \tag{5}$$

$$E_y = \frac{1}{4}\left(E_{1y} + E_{2y} + E_{3y} + E_{4y}\right) \tag{6}$$

$$E_z = \frac{1}{4}\left(E_{1z} + E_{2z} + E_{3z} + E_{4z}\right) \tag{7}$$

The locations of the electric field components on the voxel edges are shown in Figure 1. The SAR is then calculated using the conductivity σ_{voxel} and mass density ρ_{voxel} assigned to the respective voxel (Annex A).

$$SAR = \sigma_{\text{voxel}} \frac{|E_x|^2 + |E_y|^2 + |E_z|^2}{2\rho_{\text{voxel}}} \quad (8)$$

In this manner, the unique conductivity and material density which have been assigned to the voxel in the FDTD mesh are preserved. Since only the tangential components of the voxel are used in the interpolation, the material properties of the adjacent voxels or the update coefficients of the respective edges need not be regarded. The factor of 2 in the denominator of Formula (8) takes into account the use of the magnitudes of the complex E-field amplitudes.

6.2 SAR averaging

6.2.1 General

Present RF exposure standards and guidelines specify time averaged whole-body-averaged SAR limits and peak spatial-average SAR limits, neither of which shall be exceeded. The peak spatial-average SAR is usually averaged over a specified mass of tissue in a cubical volume, such as the trunk, the head, an extremity (e.g. limbs) or the pinnae. Different averaging masses may apply for body tissue and extremity tissue [1], [3]. When averaging SAR over tissue in the body, or over an extremity, only SAR values from tissues or extremities requiring the same averaging volume or mass and SAR limit shall be considered in the averaging. If any cubic volume contains tissue from the body and from an extremity, each shall be considered separately. Specifically, when determining the peak spatial-average SAR in a cube of tissue in the body, any tissue belonging to an extremity that may be contained in the cube shall be disregarded. Similarly, when determining the peak spatial-average SAR in tissues in an extremity, any tissue contained in the cube from the body shall also be treated as background material. The orientations of the cubes used for SAR averaging shall align with the coordinate axes used in the numerical computational procedures.

The regions of tissue that shall be considered as an extremity are defined by the applied RF exposure standard. The averaging algorithm follows the same definition for body tissues and extremities. The SAR averaging software shall provide appropriate means for the selection of the extremity tissues and body regions.

A procedure for the calculation of the peak spatial-average SAR is given in Annex E of [12]. However, it contains some ambiguities and open issues which can lead to inconsistent results in different implementations of the algorithm. In order to obtain consistent results in numerical SAR evaluation with different simulation tools, this document reformulates the procedure set forth in Annex E of [12]. This procedure is taken as the basis, to which minor modifications and additions are made in this document in order to address the ambiguities of flagging the states of the voxels (Table 1) and clearly define their contribution to the averaging volume. These modifications and additions are as follows.

- A definition on how to flag partially used voxels, i.e. voxels which are intersected by one or more faces of the averaging cube. These voxels shall not be flagged as “used”. The procedure in [12] was not specific in this case.
- An additional criterion for averaging around unused voxels, in the rare case that the procedure results in more than one possible averaging cube.
- A new rule that limits the maximum amount of background material (3.7) in an averaging cube. This will be limited to 10 % of background material by volume. This means that the cubical volume which is averaged about a valid voxel and consists of valid and/or used voxels shall not contain more than 10 % of background material. The mass of the background material does not contribute to the target mass.
- All faces of the cubical volumes of the valid voxels shall intersect the tissue or be entirely embedded in it. A tangential face on an interface of tissue and background material is regarded as entirely embedded in the tissue. The fraction of the background material shall be determined after the volume has reached the target mass.

- For tissue in the body, the spatial-average SAR shall be evaluated in cubical volumes that contain a mass that is within a tolerance limit of ±0,000 1 % of the target mass.

Figure 2 shows a flow chart with the most relevant steps of the algorithm. 6.2.2 defines its implementation in detail.

NOTE Interlaboratory comparison studies conducted with different implementations of the algorithm for the calculation of the peak spatial-average SAR (psSAR) have shown that a tolerance of ±0,000 1 % for the averaging mass is required to achieve consistent averaging statuses of the voxels of the SAR Star benchmark (8.2.4). While the tolerance may appear unnecessarily low, it does not represent a technical problem with respect to the implementation and does not lead to convergence problems when applying the algorithm in practical situations.

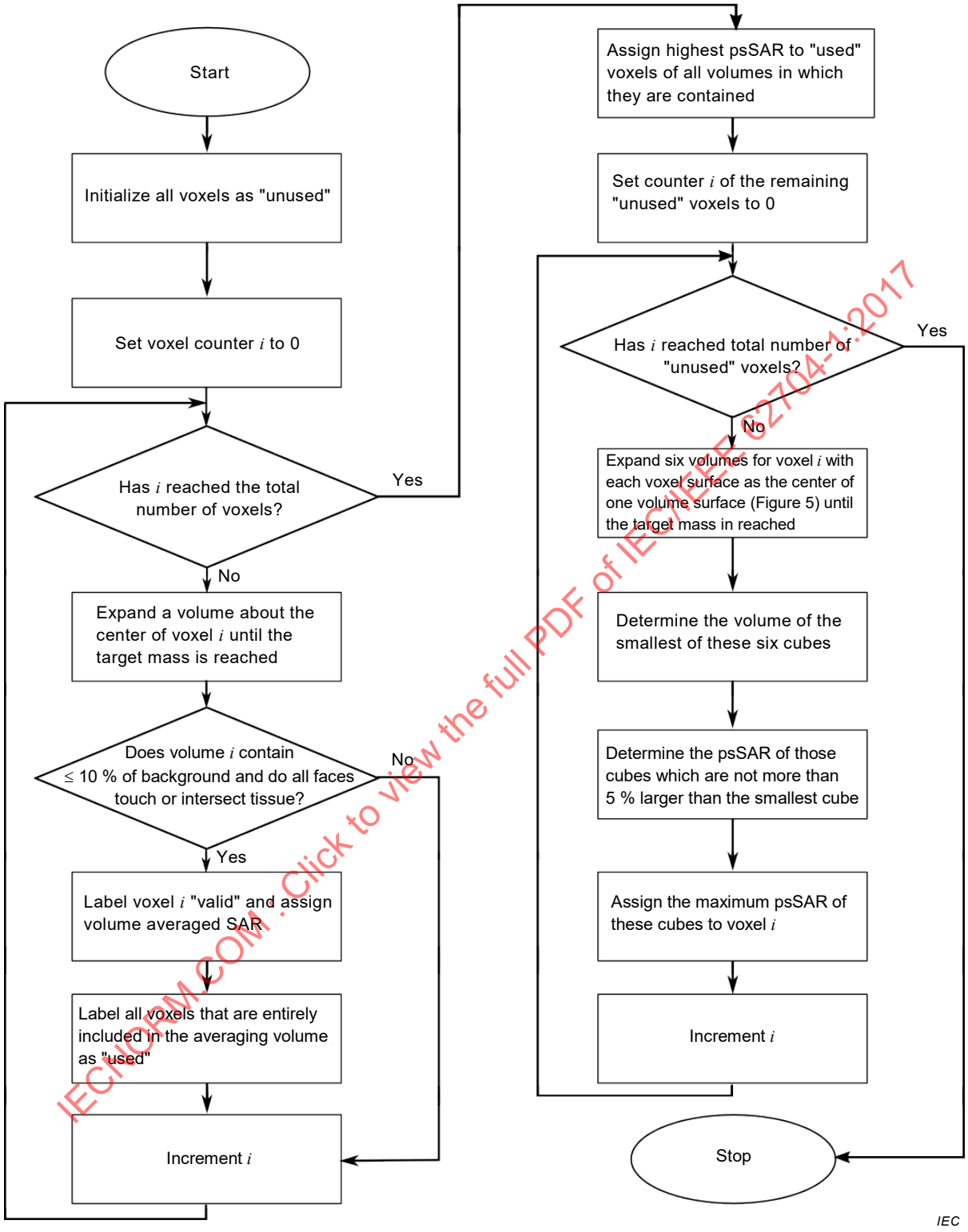

Figure 2 – Flow chart of the SAR averaging algorithm

6.2.2 Calculation of the peak spatial-average SAR

In order to determine the peak spatial-average SAR, a spatial-average SAR value is calculated for each voxel. All voxels shall be initialized with the label “unused”. In a first step, the averaging algorithm shall step through all the voxels in the body. The cubical volume centred at each voxel location, as defined above, shall be expanded evenly in all orientations ($\pm x$, $\pm y$ and $\pm z$) until the desired value for the target mass is reached. When expanding the

volume, the outermost layer of the averaging cube may require partial voxels to be considered, in order to achieve the required target mass. As a consequence, the outermost layer of voxels in an averaging cube may contain partially included voxels to achieve the required averaging mass. If the resulting cube contains less than or equal to 10 % of background material by volume (Figure 3) and all of its faces touch (for entirely contained voxels) or intersect (for partially contained voxels) the tissue, then its centre voxel shall be labelled as "valid". Otherwise, the averaging cube shall not be used to compute spatial-average SAR. During this process, reference shall be kept of all voxel locations that have entirely been included (flagged as “used”) in an averaging cube to compute the spatial-average SAR. A voxel is regarded as entirely included in the averaging volume if 99,9 % of its volume is encompassed by the cube. Spatial-average SAR values are assigned to the centre voxel location of each valid averaging cube. All voxels which are included entirely in an averaging cube shall be labelled as "used" to indicate that they have been part of at least one averaging volume. While voxels which are included partly in an averaging cube do have a partial contribution to the SAR calculation, they are not labelled as “used”. The contribution of these voxels to the spatial-average SAR shall be calculated using linear interpolation of the absorbed power, considering the fraction of their volume encompassed by the averaging volume. At the end of this first step, the voxels deep inside the body will typically be centres of valid averaging cubes, while many of the voxels near the surface will have been labelled as “used,” although no spatial-average SAR has been determined for them yet (Figure 4). Those voxels which form curved or uneven surfaces or thin parts of the body may not be included in any valid averaging volume and may therefore keep their “unused” label.

The locations that are labelled as “used” and have never been in the centre of an averaging cube shall be assigned the largest spatial-average SAR value of the averaging cubes in which they are enclosed.

For all “unused” voxel locations, new averaging cubes shall be constructed in a second step by expanding the averaging cube with individual surfaces of the “unused” voxel centred on a surface of the averaging cube. For each “unused” voxel, six averaging cubes shall be determined, each of which has the “unused” voxel centred on its surface. The other five faces of the cube shall be expanded evenly in their normal orientations until the target mass of tissue in the body is enclosed within the volume of the cube regardless of the amount of enclosed background material (Figure 5). The spatial-average SAR values of those cubes whose volume is not larger than 5 % of the volume of the smallest cube shall be preselected. The highest spatial-average SAR value of these preselected cubes shall be assigned to the “unused” voxel.

NOTE As the objective of the algorithm is to find the cube with the smallest percentage of background material for a given mass, a tolerance of 5 % on the cube size is introduced because numerical uncertainties in the calculation of the power absorbed in the voxels can lead to ambiguities in cases where more than one cube of approximately the same volume can be grown. Intercomparison studies with different implementations have shown that a tolerance of 5 % on the volume reliably identifies the maximum peak spatial-average SAR in such situations.

If the entire mass of the tissues to be averaged is less than the target mass, the peak spatial-average SAR shall be determined as the ratio of the total power dissipated in the tissues to be averaged to the entire mass of these tissues. For example, this situation can occur when averaging over the pinna of an anatomical model of a child excluding the head tissue and using an averaging cube of 10 g. The tissue masses of children’s pinnae are typically below 10 g.

When implementing the algorithm, growth of the averaging volumes beyond the boundaries of the computational domain shall be avoided as this may lead to an undefined state of the algorithm.

Table 1 – Voxel states during SAR averaging

Voxel label	Definition
unused	initial state of all voxels upon initialization of the averaging algorithm (The voxels which keep their unused status after the first step of the averaging algorithm will be used to construct cubical volumes with these voxels on the six surface layers.) Partially used voxels will not be labelled as used or valid during the first step.
used	any voxel that is entirely contained in the averaging cube of a valid voxel
valid	any voxel which is the centre of an averaging cube which contains ≤ 10 % of background material and has none of its faces completely embedded in background material

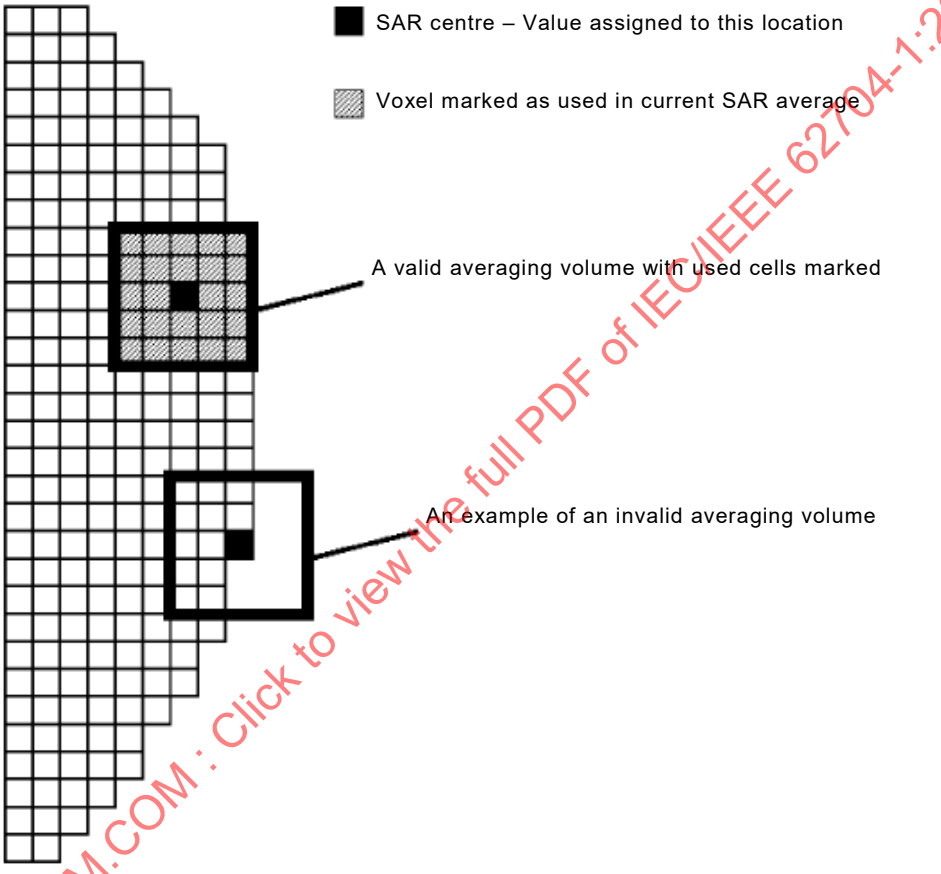

NOTE For the upper volume, the averaging cube is formed by the enclosed voxels (highlighted).

Figure 3 – Illustration of valid and used voxels in a valid averaging cube centred on the highlighted voxel and an invalid averaging volume for which a new cube has to be expanded about the surface voxel because it contains more than 10 % of background material

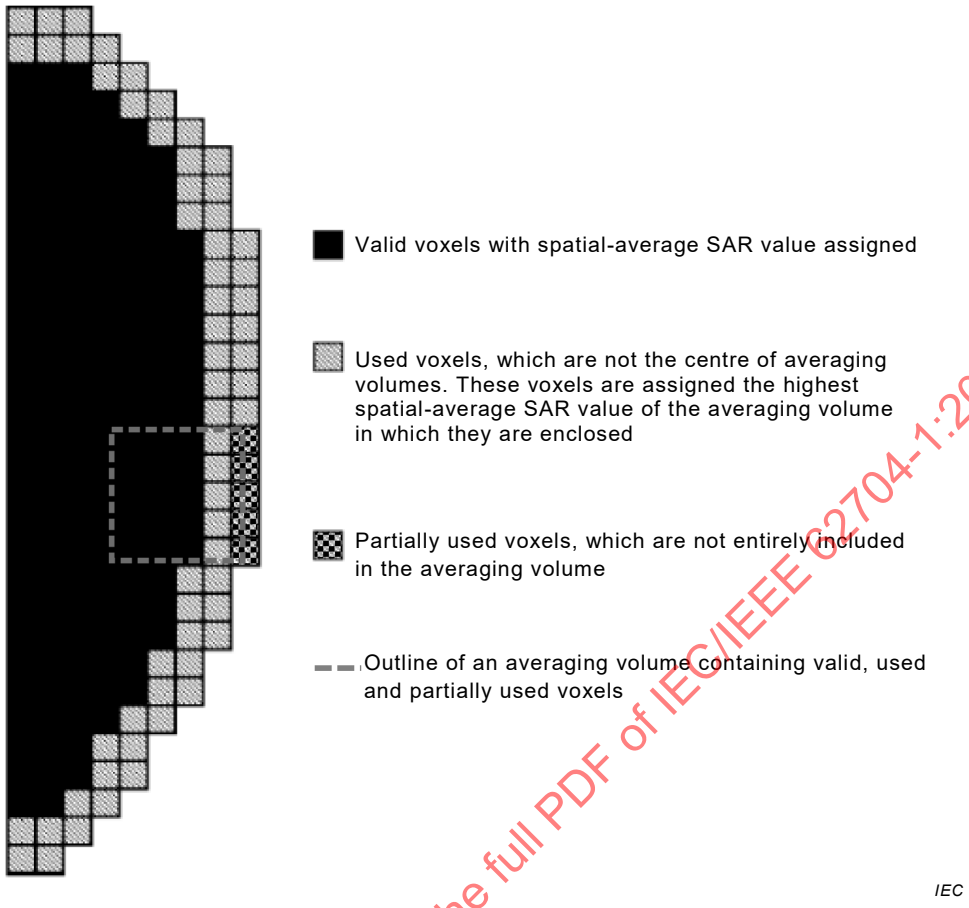

Figure 4 – Valid, used and partially used voxels

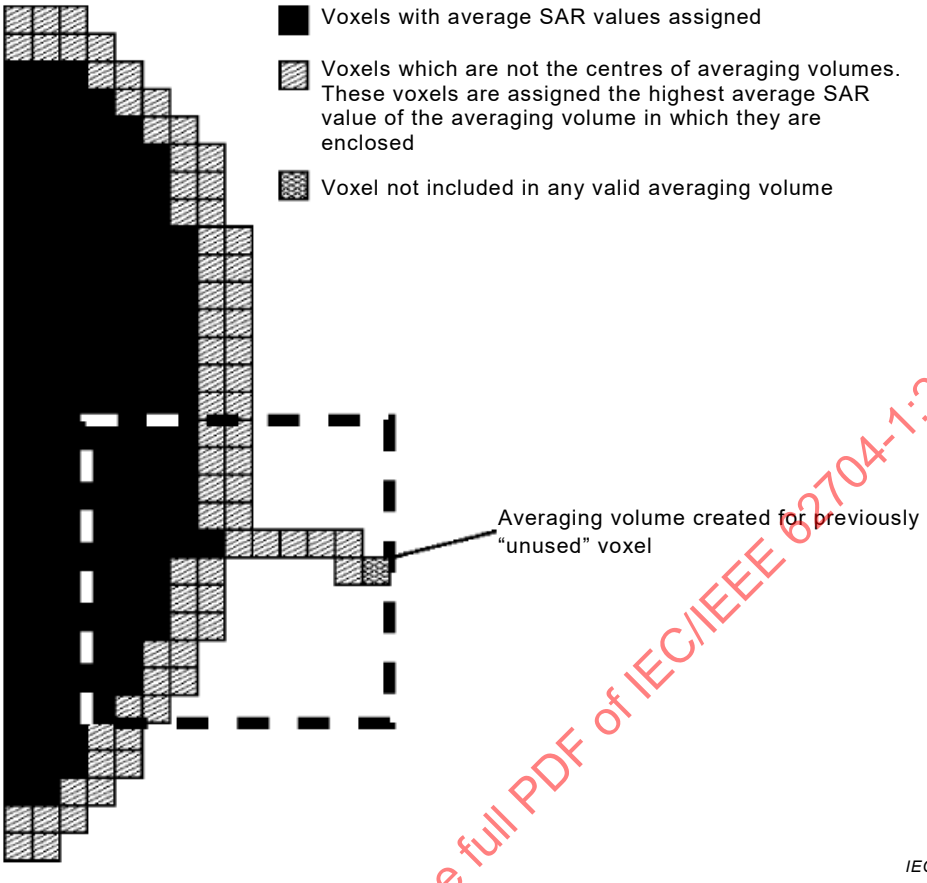

NOTE This figure shows a slice similar to the one shown in Figure 4, except for a body protrusion showing a distal "unused" voxel remaining from the first step of the averaging process. Also shown is the adjusted averaging cube created to include the previously unused voxel (centred at the exterior surface).

Figure 5 – "Unused" location

6.2.3 Calculation of the whole body average SAR

The whole body average SAR shall be calculated as the ratio of the power dissipated in all voxels consisting of tissues and fluids of the body divided by its total mass. The power dissipated in each voxel shall be calculated by multiplying the voxel SAR of Formula (8) by the voxel density ρ_{voxel}. The power dissipated in the whole body shall be calculated by summing up the dissipated power in all voxels of the body.

NOTE Possible uncertainties caused by round-off errors are considered in the evaluation of the power budget (7.2.5).

6.2.4 Reporting peak spatial-average SAR and whole body average SAR

The maximum value of the spatial-average SAR distribution, i.e. the peak spatial-average SAR, shall be reported together with its computational uncertainty for both body and extremity tissues. In addition, the coordinates of two corner points of the averaging cube shall be reported. The first corner point is defined by the minimum x-, y- and z-coordinates of all six corner points of the cube, the second corner point by its maximum x-, y- and z-coordinates. The whole body average SAR shall be reported with its computational uncertainty.

6.2.5 Referencing peak spatial-average SAR and whole body average SAR

Test results that are identified as compliant with the peak spatial-average SAR and whole body average SAR procedures of IEC/IEEE 62704-1 shall satisfy the definition of the FDTD algorithm of Clause 5 and the SAR averaging requirements of Clause 6. Moreover, the simulation software shall have passed the code verification of Clause 8. The peak spatial-

average SAR and the whole body average SAR shall be referenced both, in written publications and in the computational software as “Peak Spatial-Average SAR according to IEC/IEEE 62704-1” or “psSAR according to IEC/IEEE 62704-1”.

6.3 Power scaling

Typical FDTD calculations are excited by a voltage or current source positioned at an appropriate location in the geometry. The meshed representation of the radiating device usually will have an input impedance different from that of the actual device. As such, it is difficult to select the complex input voltage or current amplitude necessary for a given input power for the calculation. The FDTD calculation will be performed using the power delivered to the load, and the output quantities, including SAR, will be relative to this supplied power. The calculation is straight-forward and involves multiplying the SAR values by the ratio of the desired input power to the computed input power:

$$SAR_{\mathrm{s}} = SAR_{\mathrm{c}} \frac{P_{\mathrm{d}}}{P_{\mathrm{c}}} \tag{9}$$

where

P_{d} is the desired input power;

P_{c} is the power computed by the FDTD simulation;

SAR_{s} is the scaled SAR;

SAR_{c} is the SAR computed by the FDTD simulation.

For these calculations, the computed input power is the power delivered to the load by the simulation which is found from the complex voltage and current at the feed-point of the excitation source in the FDTD mesh. This is found by

$$P_{\mathrm{c}} = \frac{1}{2}\mathrm{Re}\left(UI^{*}\right) \tag{10}$$

where U and I are complex quantities. The asterisk indicates the complex conjugate. The complex values of U and I may be found from two samples of the instantaneous values of the voltage and the current at the feed-point taken one quarter-cycle of the input sine wave apart or from the DFT or FFT of the voltage and current time records of their broadband time domain signals. The two samples taken a quarter-period apart represent the real and the imaginary parts of the respective quantity. As these samples may be taken at any quarter-period during the simulation, they are affected by an undefined phase offset. This phase offset is of no relevance for all calculations described in this document and is therefore not considered any further.

If an incident plane wave source is applied, the SAR can be scaled based on the incident power density. The incident power density may be computed from

$$P_{\mathrm{inc}} = \frac{1}{2}\mathrm{Re}\left(E_{\mathrm{inc}} \times H_{\mathrm{inc}}^{*}\right) \tag{11}$$

where E_{inc} and H_{inc} represent the incident electric and magnetic fields from the plane wave. The asterisk indicates the complex conjugate. The computed incident power density can then be used to scale the SAR in the same manner as the input power.

Changes in SAR due to performance variations in RF components which affect P_{d} (due to thermal, electrical or other tolerances) shall be determined during the experimental validation of the numerical model of the DUT (7.3). It shall be considered either by choosing the maximum possible value for P_{d} or, if appropriate, by adding the performance variation in the

uncertainty budget (7.4). Details may be defined in the respective application oriented standards.

7 SAR simulation uncertainty

7.1 Considerations for the uncertainty evaluation

In experimental SAR assessment of mobile telephones, the actual unmodified physical device under test (DUT) is controlled by a base station simulator that simulates actual use. The equipment used in a SAR testing laboratory (phantom, tissue simulating materials, etc.) is developed to optimize measurement accuracy within the acceptable uncertainty range considering all the technical limitations. All factors contributing to the uncertainty are therefore well defined. The advantage of the experimental setup is that the uncertainty of the assessment is only dependent on the uncertainty of the measurement setup and independent of the DUT. In other words, the upper bound of uncertainty can be determined for the test facility such that it is valid for any DUT tested in the defined configurations.

The advantage of numerical SAR evaluation using FDTD is that it hardly poses any limitations on the test configuration, for example, numerical dosimetry allows high-resolution phantom or human body models to represent non-homogeneous tissues whereas experimental dosimetry requires strongly simplified phantoms consisting of homogenous material with rather smooth surfaces (D.3). On the other hand, numerical dosimetry requires the modelling of the DUT. Since the number of elements that could affect the near-field of devices such as cell phones is almost infinite, the intrinsic assessment of the uncertainty is practically impossible [13]. In other words, numerical SAR evaluation with known uncertainty is only possible if representative measurements of the DUT with known uncertainty are conducted in parallel. These measurements can be done with a simplified setup.

Clause 7 defines general procedures for the evaluation of the SAR simulation uncertainty which shall be conducted for each test configuration of the exposure scenario under investigation. Relevant SAR simulation standards for specific devices or applications such as IEC/IEEE 62704-2 or IEC/IEEE 62704-3 can be applied to complement the general approach taken in this document for computational and device modelling uncertainty and can provide additional definitions based on applicable rationales. The factors that contribute to the uncertainty of experimental and numerical SAR evaluation are identified in Table 2.

Table 2 – Factors contributing to the uncertainty of experimental and numerical SAR evaluation

Uncertainty factor	Experimental SAR evaluation	Numerical SAR evaluation
DUT	No additional uncertainty evaluation required for the DUT if it is tested under actual usage conditions.	The validity of a DUT model and the associated computational uncertainty shall be determined (7.3) in parallel with relevant measurements, e.g. in a simplified test setup that is representative of the actual usage conditions.
Test facility (phantom, probes, etc.)	The measurement uncertainty for the test setup is determined independently of the DUT performance tolerances. Test setup and protocol are optimized for phantom configuration, which is a function of calibration, tissue material, phantom shape, positioning tolerance, etc.	The computational uncertainties due to the test configuration (7.2) can be kept small, even for more complex configurations. Additional validations of the simulations may be required to take into account variations due to different tissue/human models and the associated exposure setup in the simulation if complex anatomical phantoms are used..
Additional validation	System performance check and validation, as required by measurement protocols, are necessary to ensure measurement accuracy and the repeatability of the measurement system.	Validation of the numerical tool is required.

In summary, the computational uncertainties are mainly related to the DUT and can be divided into the following two categories:

– uncertainty of the modelling of the DUT, such as those introduced by the simulation parameters (meshing, convergence, etc.);

– uncertainty of the numerical representation of the model of the DUT, such as those introduced by the simplification of the model (omission of parts, unknown dielectric properties, etc.).

These uncertainties concern also the modelling and the numerical representation of the phantom. All modelling and simulation work shall be carried out using a software that has been validated according to Clause 8.

7.2 Uncertainty of the test setup with respect to simulation parameters

7.2.1 General

It is recommended to define a standard way of modelling the test configuration (e.g. type and location of the absorbing boundary conditions with respect to the phantom, maximum mesh resolution for the phantom, etc.) and to determine the uncertainty parameters for ABC, mesh resolution, etc., in a generic global way that is valid for all tests of the particular setup. If, for example, the positioning of the phantom is changed when simulating different configurations, only the positioning uncertainty shall be re-evaluated provided that this change does not affect the mesh resolution of, for example, the DUT or the phantom. If, for example, a configuration change requires changes to the mesh, the mesh resolution uncertainty shall be re-evaluated, etc.

7.2.2 Positioning

For homogeneous meshes, the distance between the phantom and the DUT shall be varied by ± 1 mesh step. For inhomogeneous meshes, the mesh step shall be chosen according to the following procedure.

- Define the bounding boxes of the phantom and the DUT.
- Determine the mesh step on the side of the bounding box of the phantom facing the DUT (If the mesh step is different on the inside and of the outside of the bounding box, the minimum shall be chosen.).
- Determine the mesh step on the side of the bounding box of the DUT facing the phantom (If the mesh step is different on the inside and of the outside of the bounding box, the minimum shall be chosen.).
- Apply the minimum of these two mesh steps to vary the distance between the DUT and the phantom.

For both homogeneous and inhomogeneous meshes, either the phantom or the DUT shall be moved.

If the surfaces of the phantom and of the DUT touch one another in the default configuration, their distance shall only be increased by + 1 mesh step. Small distances larger than zero between the phantom and the DUT shall always be resolved with at least one mesh step in the default configuration in order to avoid intersections of the phantom and the DUT when reducing their distance for the evaluation of the positioning uncertainty.

The deviation of the target quantity (e.g. peak spatial-average SAR or whole body SAR) shall be reported. This value corresponds to the source and phantom separation positioning uncertainty (rectangular distribution). If the modification of the mesh step leads to unphysical intersections, for example, of the DUT and the phantom, the positioning uncertainty shall be evaluated only in the direction which does not lead to intersections.

If the target quantity (e.g. peak spatial-average SAR or whole body SAR) depends not only on the distance between the DUT and the phantom but also on positions in the other coordinate axes (e.g. in case of a strongly curved or even concave phantom), the positioning uncertainty shall also be evaluated for the other axes, following the procedure outlined here. The maximum observed deviation shall be reported.

7.2.3 Mesh resolution

The effects of refining the mesh resolution on the modelling results are the following.

a) The numerical accuracy increases with respect to dispersion and reflection/refraction.

b) The representation of the fields is improved in regions with high geometrical detail.

c) Interpolation errors of the post processor are reduced for SAR computation.

Whereas the numerical dispersion errors mentioned in a) can be regarded as negligible for SAR assessment in the human body in the near-field or the close far-field of wireless devices, provided that the considerations on the voxel size in C.2.2 are considered, the latter two outlined in b) and c) contribute significantly to the simulation results. If the computational domain encompasses several wavelengths and interference due to multiple reflections, the numerical dispersion error shall be considered as an uncertainty component.

NOTE [11] shows that the error in spatial-average SAR caused by the numerical dispersion can be kept below 3 % for tissue simulating liquids if a mesh step of 2 mm is used at 900 MHz and if the simulated domain is electrically small.

The effect of the mesh resolution shall be determined by reducing the step sizes of all axes by a factor of 2 and 4. If the simultaneous reduction of the step sizes is not possible, for example, because of memory limitations, x-, y- and z-axes shall be refined separately by a factor of 2 and 4. The deviation of the target quantity (e.g. peak spatial-average SAR or whole body SAR) for all test cases shall be reported, and the uncertainty shall be determined from the maximum deviation of all simulated cases. If the mesh axes are refined separately, the root sum square (RSS) of the maxima of each axis shall be reported. As such, the combined effects of the mesh resolution will be evaluated.

7.2.4 Absorbing boundary conditions

The impact of the ABCs depends significantly on the type of exposure scenario to be simulated and shall be determined by moving the boundaries away from the bounding box containing the original computational domain, by $\lambda/4$ separately in all coordinate directions, i.e. six simulations are required in addition to the original one. This evaluation applies to all types of ABCs. The deviation of the target quantity (e.g. peak spatial-average SAR or whole body SAR) shall be reported.

If an absorbing or reflecting object (e.g. a phantom, conducting ground or pavement) covers the entire cross section of the computational domain, i.e. spans over two dimensions, and reflections which scatter back from the boundary through this object are attenuated to 1 % or less of their original power, the spurious reflections of the ABC covered by this object need not be assessed by separate simulations. The attenuation of the reflected power shall be assessed by calculating the plane wave decay for the specific dielectric and frequency over the minimum thickness of the object. The requirement on the ABC in 7.2.4 shall be fulfilled unless there are different specific requirements defined in relevant SAR simulation standards for specific devices or applications; for example, IEC/IEEE 62704-2 or IEC/IEEE 62704-3.

7.2.5 Power budget

The power fed into the computational domain shall be recorded at the sources (source power). The sum of the power absorbed in the lossy dielectrics in the computational domain and radiated into the ABCs shall be recorded and compared to the source power. Depending on numerical uncertainties, such as poor convergence or roundoff errors, the sum of the absorbed and the radiated power will not be precisely equal to the source power, and it is not possible to determine where power is spuriously dissipated or generated. Since a linear relationship exists between SAR and power, the error of the power budget is directly proportional to the SAR uncertainty. The deviation shall be reported as uncertainty (normal distribution).

When simulating devices with multiple sources operating simultaneously, the correct loading of all ports has to be asserted. It is recommended to excite each port separately while loading the inactive ports with the reference impedance in order to compute the full S-matrix of the multiport system. As such, the SAR and the total power budget for a given excitation vector can be calculated by superimposing the fields for any excitation vector and load. For details refer to, for example, [14], [15], [16], [17] or [18].

7.2.6 Convergence

7.2.6.1 Harmonic simulations

The E-field vector components shall be recorded in the time domain in the region where the target quantity (e.g. peak spatial-average SAR or whole body SAR) is expected. The absolute value of the vector shall be calculated at each time step. For a sufficiently converged simulation, the deviation of the last three local maxima of the squared absolute values of the E-fields from their mean value shall not be larger than 2 %, and the maxima shall be found in the same voxel. If the simulation cannot be run for a sufficient time to reach a deviation of less than 2 %, a rationale shall be given in the test report explaining why a relaxed tolerance can be used for the particular application under test to rule out incorrectly configured simulations, i.e. to which extent the convergence contributes to the target quantity. The deviation shall be reported as uncertainty with rectangular probability distribution. Since the location of the target quantity may not be known a priori, it is recommended to record the time domain signal at several locations in order to avoid repeated simulations. Testing simulations with coarser meshes or simplified geometry may help to limit the computational expenses to identify the relevant regions for the recording of the signals.

7.2.6.2 Time domain simulation with Fourier transformation

For broadband simulations with evaluation of the target quantity (e.g. peak spatial-average SAR or whole body SAR) by Fourier transformation, a signal with a pulse shaped envelope is

used for excitation. The E-field components shall be recorded as described in 7.2.6.1. If the target quantity is evaluated at several frequencies, frequency dependent changes in location of the target quantity shall be considered. For the evaluation of the uncertainty, the discrete Fourier transform of the time domain signal shall be calculated for increasing windowing lengths t_w starting at $t_0 = 0$ and ending at $t_w = 1{,}25\,nT$. T is the period of the evaluation frequency and n is an integer number which shall be increased until t_w reaches the end of the simulated time or until the convergence limit has been reached. The deviation of the last two squared absolute values of the DFT results at the evaluation frequency from their mean value shall not be larger than 2 % for a sufficiently converged simulation. If the simulation cannot be run for a sufficient amount of time to reach a deviation of less than 2 %, a rationale shall be given in the test report explaining why a relaxed tolerance can be used for the particular application under test to rule out incorrectly configured simulations. The deviation shall be reported as uncertainty with rectangular probability distribution.

7.2.7 Dielectrics of the phantom or body model

The dielectric parameters of the tissues or tissue simulating material of the phantom or body model are usually affected by uncertainties according to their specification data sheet publication. Further information can be found in Annex D. The impact of these uncertainties on the peak spatial-average SAR shall be evaluated by applying the minimum and maximum conductivity and permittivity (four different combinations). The minimum and maximum shall be chosen according to the uncertainty that is reported by the source of the dielectric parameters, e.g. data sheet, publication. In order to avoid excessive numbers of simulations for structures with a large number of different dielectrics, the changes in conductivity and permittivity may be limited to the region where most of the electromagnetic energy is confined or absorbed, or advanced statistical methods may be applied for the quantification of the uncertainty. In such cases, an appropriate rationale shall be given.

Dielectric parameters for certain reference phantoms or models may be specified with an uncertainty of zero. In this case, no additional evaluations are required, and the corresponding entry in Table 3 shall be set to zero. The maximum deviation from the peak spatial-average SAR obtained using the nominal value of the permittivity and conductivity shall be reported.

Table 3 – Budget of the uncertainty contributions of the numerical algorithm and of the rendering of the test- or simulation-setup

a	b	c	d	e	f	g	h
Uncertainty component	**Subclause**	**Tolerance %**	**Probability distribution**	**Divisor f(d, h)**	c_i	**Uncertainty %**	v_i or v_{eff}
Positioning	7.2.2		R	1,73	1		
Mesh resolution	7.2.3		N	1	1		
ABC	7.2.4		N	1	1		
Power budget	7.2.5		N	1	1		
Convergence	7.2.6		R	1,73	1		
Phantom dielectrics	7.2.7		R	1,73	1		
Combined standard uncertainty (k = 1)							

Columns c, g and h shall be filled in based on the results of the DUT simulations.

NOTE 1 Column headings a to h are given for reference.

NOTE 2 Abbreviations used in Table 3:

N, R – normal, rectangular probability distributions

NOTE 3 The divisor is a function of the probability distribution and degrees of freedom (v_i and v_{eff}).

NOTE 4 c_i is the sensitivity coefficient that is applied to convert the variability of the uncertainty component into a variability of SAR.

7.3 Uncertainty and validation of the developed numerical model of the DUT

7.3.1 General

The goal of 7.3 is to assess simulation uncertainty contribution related to the accuracy of the DUT modelling, with respect to the SAR induced in the exposed phantom. Among other parameters, the evaluated SAR depends on current distribution in the DUT and therefore has an uncertainty associated with the limited accuracy due to simplifications introduced to a CAD-based DUT model. The level of details necessary to develop an accurate numerical model of a real device and the evaluation of its uncertainty depend on the testing or exposure assessment configurations. Many exposure conditions include the DUT in close proximity to the exposed object with some degree of interaction between them. This interaction can be accounted for by the FDTD method. In general, to properly account for this interaction, it is important not to define a fixed distribution of the RF currents on the DUT model, for example, by using a set of distributed current sources or by forcing H-fields to a particular value in the solver software. The antenna feed-point(s) of the DUT model shall be fed by one or more sources which ensure that the contributions of all parts of the DUT which contribute to the RF current distribution be appropriately reproduced. The accuracy of this model shall be evaluated by comparing the measurements and the simulations of the electromagnetic fields generated by the DUT at specific reference locations.

In some cases, when the DUT is represented by a numerical model with predefined current distribution or approximations based on, for example, the Huygens box technique [8],[19], the interaction between the DUT and the phantom is not considered by the numerical algorithm, although it could be significant at close separation distances. For those models the uncertainty of the DUT shall include interaction effects using the approach described in 7.3.2.

In order to isolate the uncertainty of the DUT model from other uncertainty contributions as much as possible and to reduce the potential differences between the measurement setup and simulation model for the purpose of uncertainty evaluation, the reference test configuration should be limited to those details which are essential for the characterization of the RF transmission and of the exposure characteristics during normal operation of the DUT. If the output power cannot be determined, for example, by measurements of the conducted power, the test conditions, such as RF channels or duty factors, shall be chosen with respect to the maximum output power following product specifications, applied wireless technology, etc. The number of tests required for the following cases is minimized and the test configurations are simplified according to the closest distance d between the DUT and the phantom.

– $d \geq \lambda/2$ or $d \geq 200$ mm: Under such exposure conditions, electromagnetic field measurement techniques developed for exposure assessment are applicable and practical, for example, [20].

– $d < \lambda/2$ and $d < 200$ mm: Under such exposure conditions, developed SAR measurement techniques are applicable and practical (IEC 62209-1 and IEEE Std 1528).

The uncertainty for these cases shall be determined with the methods described in 7.3.2 and 7.3.3.

7.3.2 Uncertainty of the DUT model ($d \geq \lambda/2$ or $d \geq 200$ mm)

Where no accurate reference field distribution is available, such as an analytical solution, it is sufficient to experimentally verify the field generated by the DUT at a distance no further than the distance at which the exposure is evaluated. The electric and magnetic field shall be scanned along a line parallel to the axis of the body of the device or subsystem that contains the antenna and radiating structures, whichever is more representative and conservative for the exposure condition under evaluation, in steps no greater than $\lambda/4$ or 100 mm (whichever is less) and compared to the numerical values. At least three points overlapping the device dimension and one point extending beyond the device dimension shall be scanned. If scattering, for example, from conducting ground cannot be excluded due to limitations of the testing environment, the scatterers shall be modelled in the numerical simulations of the DUT. If such scatterers are included in the test setup, at least two different distances in steps of $\lambda/4$

between them shall be measured and simulated, where at least one of these measurement distances shall be less than the exposure distance. The SAR uncertainty, based on a rectangular probability distribution, shall be assessed as the maximum deviation of the square of the field components normalized to the maximum experimental value, using

$$U_{\mathrm{SAR}}[\%] = 100 \times \mathrm{MAX}\left(\frac{\left| E_{\mathrm{ref}}^2(n) - E_{\mathrm{num}}^2(n) \right|}{E_{\mathrm{refmax}}^2}, \frac{\left| H_{\mathrm{ref}}^2(n) - H_{\mathrm{num}}^2(n) \right|}{H_{\mathrm{refmax}}^2} \right) \quad (12)$$

where

U_{SAR} is the uncertainty in percent;

E_{ref} is the experimentally determined incident electric field value at location n or its accurate reference solution;

H_{ref} is the experimentally determined incident magnetic field value at location n or its accurate reference solution;

E_{num} is the numerically determined incident electrical field value at location n;

H_{num} is the numerically determined incident magnetic field value at location n;

$E_{\mathrm{ref\ max}}$ is the maximum of the experimentally determined incident electric field value of all measured locations or its accurate reference solution;

$H_{\mathrm{ref\ max}}$ is the maximum of the experimentally determined incident magnetic field value of all measured locations or its accurate reference solution.

For a DUT which is mounted on a ground plane, the reference ground plane shall be used to represent the intended operating conditions. In cases where regions below the ground plane are inaccessible and there is no exposure concern, the reference points for the electromagnetic field measurements and simulations shall be located above the ground plane.

If the DUT is approximated by a model with a fixed predefined distribution of the RF currents, using the Huygens box technique or any other equivalent method where the incident field generated by the DUT model is predetermined and does not change due to possible interaction with a phantom, the accuracy of such approximation shall also be evaluated if the exposed body is within one wavelength or a distance of 2 m (whichever is less) from the antenna. In this case the DUT uncertainty evaluation shall be based on magnetic field measurements that involve the DUT loaded by the human body (phantom) in the SAR evaluation configuration. The measurements shall be conducted using an H-field probe in the closest vicinity of the antenna between the DUT and the exposed human body (phantom) and compared to the numerical values computed for the same condition. At least 10 points overlapping the device dimension and one point extending beyond the device dimension shall be scanned. The distance between these points shall be no larger than a quarter of the wavelength, and the locations of the H-field maxima for the measured and simulated exposure conditions shall also be reported and verified to be the same. The SAR uncertainty based on a rectangular probability distribution shall be assessed as the maximum deviation of the square of the measured field magnitudes normalized to the maximum experimental value:

$$U_{\mathrm{SAR}}[\%] = 100 \times \mathrm{MAX}\left(\frac{\left| H_{\mathrm{ref}}^2(n) - H_{\mathrm{num}}^2(n) \right|}{H_{\mathrm{refmax}}^2} \right) \quad (13)$$

NOTE The applicability of the Huygens box technique to near field exposure has been demonstrated, for example, for birdcage resonators used in magnetic resonance imaging [21].

The measurements required for these evaluations shall be conducted with instrumentation that minimizes the perturbation of the measured fields for more reliable comparison with the simulation results. Depending on the physical dimensions of the field sensors used, there may be inherent spatial averaging over the region occupied by the field sensors. This can lead to

larger discrepancies between the measured and simulated field results. It is recommended that miniature E-field and H-field probes/sensors be used to keep the uncertainty of the comparison to the minimum. The reference documentation of the applied instrumentation and/or appropriate measurement standards, describing the specific application of this general approach, should provide sufficient details to help ensure high quality of the reference configuration setup. Their uncertainties shall be determined appropriately. The uncertainty of the developed model of the DUT shall be evaluated according to Table 4.

7.3.3 Uncertainty of the DUT model ($d < \lambda/2$ and $d < 200$ mm)

In the reactive near-field of the source, the coupling of the fields directly with the body may have a strong effect on the transmitter. In this case, the only way to determine the uncertainty of the DUT model is by SAR measurements. In such a case, the uncertainty of the phantom model contributes to the uncertainty of the model of the DUT. However, simplified measurements can be used. It is recommended to use a flat phantom for the measurements because the uncertainty of the numerical model of such a phantom is expected to be negligible, such that a particular evaluation of the phantom uncertainty is not necessary.

Otherwise, the phantom uncertainty shall be assessed separately by applying the procedure defined in 7.2 on the phantom instead of the DUT. The objective of this evaluation is the assessment of the numerical representation of more complex phantom shapes or inhomogeneous dielectrics. As the evaluation is carried out numerically, all entries of Table 3 shall be evaluated separately for the phantom with the exception of the evaluation of the positioning uncertainty (7.2.2). The uncertainty evaluation for these entries of Table 3 shall be conducted for exposure to incident plane waves from all orthogonal directions of the coordinate system (e.g. front, back, left, right, top, bottom) and two orthogonal polarizations of the incident E-field vector for each direction (12 evaluations). The maximum uncertainty value of these 12 evaluations shall be used as the phantom uncertainty.

In order to determine the effect of backscattering, different distances between the DUT and the phantom shall be evaluated in order to take into account different loading conditions. The uncertainty shall be determined by assessing the deviation of the SAR amplitude and distribution for three different distances. The default distance d_0 between DUT and phantom shall be the same as the one required by the SAR simulation. In most cases this will be the distance of the intended use as specified by the manufacturer or by the relevant measurement standards, for example, IEEE Std 1528. This distance shall lie within the $d < \lambda/2$ and $d < 200$ mm range. The other two distances to be evaluated are $0{,}5\,d_0$ and $1{,}5\,d_0$. If the default distance d_0 is zero, the DUT shall be evaluated at zero, at the maximum of the $d < \lambda/2$ and $d < 200$ mm range (whichever is less) and at 10 % of this maximum. If the distance of $1{,}5\,d_0$ exceeds the maximum of the $d < \lambda/2$ and $d < 200$ mm range (whichever is less) by more than 30 %, a distance of $0{,}75\,d_0$ shall be evaluated instead. If the SAR levels at the larger distances are too low to be measured with sufficient accuracy (e.g. due to noise), two alternative distances shall be evaluated at which the SAR level shall be sufficiently high above the noise level and at which different characteristics of the incident field (near- and far-field range) should be covered. A rationale for these distances shall be given.

The uncertainties shall be determined by the experimental and numerical assessment of the SAR distribution for the three different separation distances between the DUT and the phantom, as described above, on a mesh with steps no larger than 15 mm or $\lambda_D/2$ (whichever is less considering the reduced wavelength λ_D in the dielectric) at no less than 100 points in a volume as close as possible to the volume containing the SAR maximum. The cross section of the volume shall entirely cover the surface of the device that faces the phantom. At least two parallel planes shall be measured. The mesh step refers to the measurement mesh. For the numerical evaluation, a finer mesh is generally required. At each distance d, the SAR uncertainty is evaluated according to

$$U_{\mathrm{SAR},d}[\%] = 100 \times \mathrm{MAX} \frac{\left| SAR_{\mathrm{ref}}(n) - SAR_{\mathrm{num}}(n) \right|}{SAR_{\mathrm{refmax}}} \tag{14}$$

where

SAR_{ref} is the experimentally determined local (unaveraged) SAR value at position n or its accurate reference solution;

SAR_{num} is the numerically determined local SAR value at position n;

$SAR_{ref\ max}$ is the experimentally determined maximum SAR value of all measured positions or its accurate reference solution.

Only the maximum SAR uncertainty of the three distances shall be reported. The reference documentation of the applied instrumentation and/or appropriate measurement standards, describing the specific application of this general approach, should provide sufficient details to help ensure high quality of the reference configuration setup. Their uncertainties shall be determined appropriately following the procedures described in IEC 62209-1 and IEEE Std 1528. The uncertainty of the developed model of the DUT shall be evaluated according to Table 4.

Table 4 – Budget of the uncertainty of the developed model of the DUT

a	b	c	d	e	f	g	h
Uncertainty component	**Subclause**	**Tolerance %**	**Probability distribution**	**Divisor f(d, h)**	c_i	**Uncertainty %**	v_i **or** v_{eff}
Uncertainty of the DUT model (incident near- or far-field distribution with or without dependence on the load)	7.3.2 or 7.3.3		N	1	1		
Uncertainty of the phantom model, i.e. of the absorption and of the backscattering (if applicable)	7.3.3		N	1	1		
Uncertainty of the measurement equipment and procedure	According to manufacturer specification and/or applied methodology		N	1	1		
Combined standard uncertainty (k = 1)							

Columns c, g and h shall be filled in based on the results of the DUT simulations.

NOTE 1 Column headings a to h are given for reference.

NOTE 2 Abbreviations used in Table 4:

N – normal probability distribution

NOTE 3 The divisor is a function of the probability distribution and degrees of freedom (v_i and v_{eff}).

NOTE 4 c_i is the sensitivity coefficient that is applied to convert the variability of the uncertainty component into a variability of SAR.

7.3.4 Model validation

The following steps shall be followed for the validation of the model.

a) Determine the uncertainty budget of the numerical model U_{sim} by evaluating the SAR uncertainty of the numerical model of the setup of 7.3.2 or 7.3.3 according to Formula (12), (13) or (14).

b) Determine the uncertainty budget of the measurement evaluation U_{ref}.

c) Validate whether the deviation between the measured SAR value at point n, v_{ref_n} (or its accurate reference), and the simulated SAR value v_{sim_n} is within the combined uncertainty of U_{ref} and U_{sim} by evaluating

$$E_n = \sqrt{\frac{\left(v_{\mathrm{sim}_n} - v_{\mathrm{ref}_n}\right)^2}{\left(v_{\mathrm{sim}_n} U_{\mathrm{sim}(k=2)}\right)^2 + \left(v_{\mathrm{ref}_n} U_{\mathrm{ref}(k=2)}\right)^2}} \leq 1 \qquad (15)$$

If E- or H-field strengths are determined in the DUT model uncertainty simulations and measurements instead of SAR, these values shall be squared to calculate the respective v_{ref_n} and v_{sim_n}.

The validation according to Formula (15) shall be carried out at every point n that is larger than 5 % of the maximum measured or simulated value $\underset{n}{\mathrm{MAX}}\left(v_{\mathrm{sim}_n}; v_{\mathrm{ref}_n}\right)$.

If the deviation is within the combined uncertainty, i.e. if $E_n \leq 1$ for any considered point, the combined standard uncertainty in Table 4 is the uncertainty for the DUT model. If the deviation is not within the expected uncertainty, the DUT model is not valid and shall be revised.

7.4 Uncertainty budget

The total numerical uncertainty budget shall be calculated from the contributions of Table 3 and Table 4 and shall be summed up as shown in Table 5. The minimum achievable uncertainty depends on the level of detail to which a particular exposure situation can be modelled. Large uncertainties may apply, for example, on the dielectric parameters of the DUT or of an anatomical phantom (D.2). While large uncertainties may be acceptable in particular situations, several studies have shown that the deviations of the numerical and experimental results can usually be kept under 30 % [22], [23], [24]. Particular tolerances may be defined in the respective SAR simulation standards and application oriented guidelines based on this document.

NOTE Additional studies applying a combined numerical and experimental approach for SAR assessment with uncertainty evaluation are, for example, [21], [25]. [22] and [23] do not assess the uncertainties of the numerical results they present, but just compare them to experimental data. [24] reports a numerical uncertainty of 9,0 % for the numerical assessment and 22,1 % for the experimental evaluation (both k = 2) of the 1 g psSAR of a generic cell phone. [21] and [25] evaluate the tissue heating in a medical application. In [21], a combined numerical and experimental uncertainty of 244 % (k = 2) is reported for the entire evaluation. [25] shows that a reduced total combined uncertainty of 20 % (k = 2) can be achieved for a similar application under well controlled conditions.

Table 5 – Numerical uncertainty budget

a	b	c	d	e	f	g	h
Uncertainty component	**Subclause**	**Tolerance %**	**Probability distribution**	**Divisor f(d, h)**	c_i	**Uncertainty %**	v_i or v_{eff}
Uncertainty of the test setup with respect to simulation parameters	7.2		N	1	1		
Uncertainty of the developed numerical model of the test setup	7.3		N	1	1		
Combined standard uncertainty (k = 1)							
Expanded standard uncertainty (k = 2)							

Columns c, g and h shall be filled in based on the results of Table 3 and Table 4.

NOTE 1 Column headings a to h are given for reference.

NOTE 2 Abbreviation used in Table 5:

N – normal probability distribution

NOTE 3 The divisor is a function of the probability distribution and degrees of freedom (v_i and v_{eff}).

NOTE 4 c_i is the sensitivity coefficient that is applied to convert the variability of the uncertainty component into a variability of SAR.

8 Code verification

8.1 General

Clause 8 provides procedures for the following two levels of code verification:

- code accuracy;
- canonical benchmarks.

An implementation of an FDTD code can be validated by the manufacturer according to the benchmarks defined in Clause 8. A code that has passed all code accuracy and canonical benchmark tests can be labelled as “Compliant with IEC/IEEE 62704-1”. The objectives of the different levels of verification are described below.

The verification of the code accuracy provides methods to determine whether the FDTD algorithm has been implemented correctly and works accurately within its numerical constraints. Additionally, the methods are used to determine the accuracy and validity of the original Yee-algorithm, such as the numerical modelling of dielectric interfaces, ABCs and certain parts of the post processing algorithms. In addition, the methods can directly be applied on the assessment of the performance of special techniques, such as subcell models for the approximation of tilted boundaries, small structures, submesh techniques, etc. Deviations from the implementation of the finite-difference time-domain method as defined in Clause 5, or from the SAR calculation as defined in 6.1, are regarded as special techniques if they are applied on the entire computational domain, on subdomains or merely on one or more edges of the mesh. Examples of special techniques can be found in [26], [27]. All canonical benchmarks can be compared to analytical solutions of the physical problem or its numerical representation. These methods characterize the implementation of the FDTD algorithm in a very general way. They are defined such that it is not possible to tune the

implementation for a particular benchmark or application without improving the overall quality of the code.

The canonical benchmarks assess the cumulative accuracy of a code and its applicability considering the interaction of its different modules, such as mesh generation, computational kernel, representation of sources, data extraction algorithms of the post processor, etc.

All benchmarks of Clause 8 shall be carried out with a three-dimensional implementation of the FDTD algorithm. Some benchmarks require the use of PEC, PMC or periodic boundary conditions.

Dimensions in millimetres

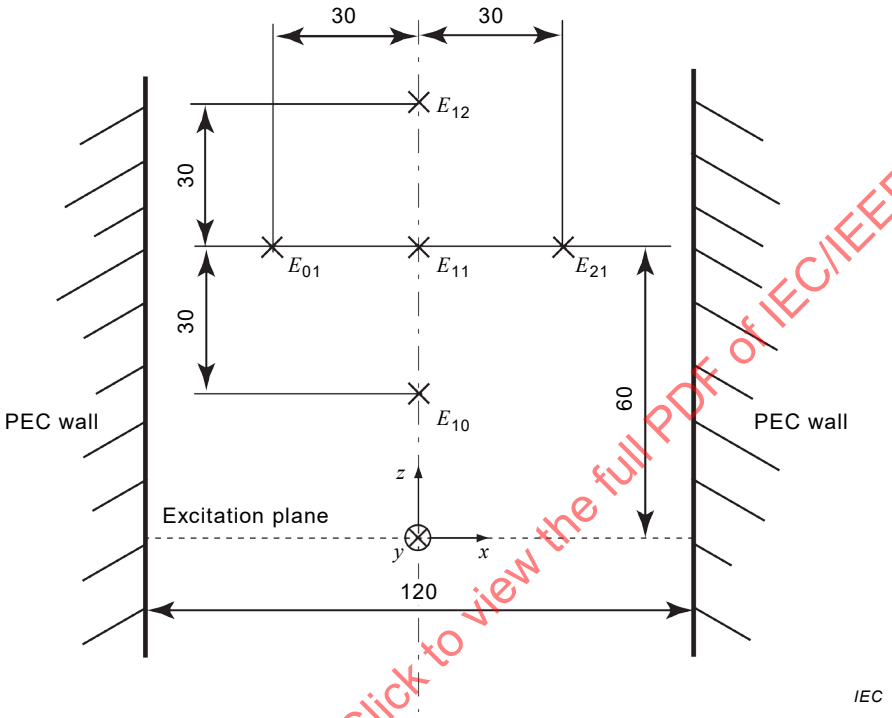

For TM-polarization, the indicated location correspond to the E_x or the E_z components, which are shifted by half a mesh step size.

Figure 6 – Aligned parallel-plate waveguide and locations of the E_y field components to be recorded for TE-polarization

8.2 Code accuracy

8.2.1 Free space characteristics

8.2.1.1 General

The assessment of the free space characteristics of a code provides the means to validate the basic implementation of the Yee-algorithm, time step calculation, dielectric materials and parameters, etc. The free space characteristics are described by the theoretical dispersion analysis of the Yee-algorithm [28] and define the numerical wave number as a function of the ratio of the voxel size to the wavelength, the time step (Courant factor) and the direction of propagation. Just like Maxwell's equations, the Yee-algorithm allows the decoupling of the solutions in independent TE and TM polarized waves. The extraction of the numerical wave number as a function of these parameters and polarizations is possible by simulating the dispersion characteristics of a parallel-plate waveguide excited with the fundamental TE and TM modes. Broadband excitation will allow the calculation of the dispersion properties of the numerical representation of the dielectric in the waveguide as a function of the frequency and the direction of propagation, including the reactive part of the plane wave spectrum. The fundamental TE and TM modes of the waveguide can be represented in the two-dimensional

formulation of the FDTD algorithm. Therefore, the waveguides can be modelled as two-dimensional structures. The waveguide modes can be thought of as a superposition of two symmetrical plane waves which change their angle of propagation as a function of the frequency. Like this, the numerical characteristics of the algorithm can be evaluated as a function of the direction of propagation, including reactive waves, if the waveguide is operated below its cut-off frequency. It should be noted that the frequency range of the benchmarks is defined such that a large range of directions is considered. It therefore does not test the code for a particular frequency range, but for a range of angles of propagation with respect to the mesh. The waveguides are meshed with homogeneous (equidistant) and inhomogeneous (graded) meshes. For the complete evaluation, the waveguides shall be oriented in all three coordinate axes and rotated around the axes (six simulations for each polarization and mesh). The deviation of the dispersion characteristics calculated from the simulation results due to numerical dispersion of the Yee-algorithm shall not be larger than ±2 %, if a homogeneous mesh is used.

Enhanced methods or special techniques which deviate from the formulation of the Yee-algorithm as defined in Clause 5 shall be validated in addition if they are used for the evaluation of a particular testing configuration. An enhancement of FDTD algorithm which yields a reduced numerical dispersion error in comparison to the original Yee-algorithm is permitted. The applied enhancement of the FDTD algorithm shall be documented (e.g. by describing the definition of the update coefficients or modifications of the update equations).

For inhomogeneous meshes, a closed solution for the numerical dispersion cannot be given. The numerical dispersion calculated for the inhomogeneous mesh shall therefore not deviate from the physically correct value by more than ±10 %. In the following, the waveguides, their excitations, data recording, extraction and the calculation of the numerical wave numbers for comparison with the analytical results will be described.

8.2.1.2 Definition of the parallel-plate waveguides

The waveguides are defined as two-dimensional structures terminated with perfectly conducting walls (Figure 6). The width in the x-direction is w =120 mm. All directions and dimensions correspond to the coordinate system as defined in Figure 6.The excitation is placed perpendicular to the orientation of the waveguide at z_0 = 0. The distance from the source to the fields to be recorded shall be 60 mm. The length of the waveguide should be chosen such that reactive fields which may be caused by the truncation of the computational domain do not reach the region where the fields are recorded. The discretization in the y-axis, which is required because of the implementation of the FDTD algorithm in three dimensions, affects the numerical dispersion only indirectly by the calculation of the simulation time step Δt to update the fields. The time step Δt is required when comparing the simulation results with the theoretical numerical dispersion (8.2.1.10).

8.2.1.3 TE polarization

For the fundamental TE mode, the waveguide shall be terminated with perfect electrical conductors (PEC) as boundary conditions in the x-direction. The E_y components at the source location (Figure 6) shall be excited with the analytical solution of the TE_1 mode. It is recommended to excite the mode with a hard source. A hard source enforces a particular E-field strength on a mesh edge [8]. This E-field strength is proportional to the excitation signal. The mode can be excited by setting the E_y components at the source location (Figure 6) to the values calculated from

$$E_y = E_0 \sin\frac{m\Delta s\pi}{w} \tag{16}$$

where

E_0 is an arbitrary E-field amplitude;

m is the index of the source component;

Δs is the mesh step;

w is the width of the waveguide.

For inhomogeneous meshes, the expression $m\Delta s$ in Formula (16) shall be replaced by the centre of the respective primary mesh edge.

Alternative methods for the field excitation may be used, such as particular solvers to determine the propagating modes in the waveguide or preconfigured sources if the software provides them. In any case, it shall be asserted that only the fundamental propagating mode exists at the location where the fields are recorded (Figure 6) because the presence of higher order modes or spurious modes hinders the evaluation of the propagation constant.

8.2.1.4 TM polarization

For the fundamental TM mode, the waveguide shall be terminated with perfect magnetic conductors (PMC) as boundary conditions in the x-axis. The fundamental TM mode for this configuration is the TM_1 mode. The mode can be excited by setting the E_x components at the source location (Figure 6) to the values calculated from

$$E_x = E_0 \cos\frac{(m-0{,}5)\Delta s\pi}{w} \tag{17}$$

where

E_0 is an arbitrary E-field amplitude;

m is the index of the source component;

Δs is the mesh step;

w is the width of the waveguide.

For inhomogeneous meshes, the expression $m\Delta s$ in Formula (17) shall be replaced by the centre of the respective primary mesh edge.

Alternative methods for the field excitation may be used, for example, such as particular solvers to determine the propagating modes in the waveguide or preconfigured sources if the software provides them. In any case, it shall be asserted that only the fundamental propagating mode exists at the location where the fields are recorded (Figure 6) because the presence of higher order modes or spurious modes hinders the evaluation of the propagation constant. Instead of the E-field components, the H-field components can be used.

8.2.1.5 Homogeneous mesh

For the simulations of the homogeneous mesh, the mesh step is 10 mm in the x- and in the z-direction. The mesh step in the y-direction may be determined by the user. It should be considered that it has an impact on the time step calculation.

8.2.1.6 Inhomogeneous mesh

The following mesh lines shall be used for the x- and z-direction: 0,0 mm; 0,5 mm; 1,4 mm; 3,1 mm; 6,3 mm; 12,0 mm; 15,0 mm; 18,0 mm; 22,7 mm; 30,0 mm; 45,0 mm; 52,5 mm; 60,0 mm and 75,0 mm. For the remaining part of the geometry, a constant mesh step of 15 mm shall be used. In the x-direction, these lines refer to the left boundary of the waveguide (x = −60 mm), and in the z-direction they refer to the origin of the coordinate system (z = 0) as indicated in Figure 6. The mesh steps cover a range from 0,5 mm to 15 mm. Like this, the simulation time step is reduced, which increases the numerical dispersion error in the larger mesh cells [10]. The origin of the x-axis is one of the waveguide walls, the origin of the z-axis is the location of the source (Figure 6). The mesh step in the y-direction, which is required because of the implementation of the FDTD algorithm in three dimensions, can be determined by the user. It should be considered that it has an impact on the time step calculation.

8.2.1.7 Excitation

The TE and TM modes of 8.2.1.3 and 8.2.1.4 shall be used as excitations for the waveguide. The signal $f(t)$ shall be sinusoidal with a Gaussian envelope which covers a frequency range from 500 MHz to 2 GHz. The frequency range covers both the reactive and the propagating range of the TE and TM modes in the waveguide and is therefore appropriate to characterize the numerical dispersion. The signal is defined as

$$f(t) = \sin(\omega_0 t)\exp\left\{\left[(t - t_0)/\tau\right]^2\right\} \tag{18}$$

The following parameters are suggested for the simulations:

$\omega_0 = 2\pi f_0 = 2\pi$ 1 250 MHz

t_0 = 1 ns

τ = 0,2 ns

NOTE The suggested centre frequency of the broadband signal ω_0 is the centre of the frequency range to be evaluated (500 MHz to 2 GHz). The bandwidth of the signal is sufficiently large to provide enough energy over the entire frequency range although its centre frequency is close to the cut-off of the waveguides.

The simulation time shall be chosen such that the remaining ripple on the recorded signals is less than 0,1 % of the source signal amplitude. The ripple shall be calculated from the maximum value of the signal within the last 5 % of the simulation time divided by the largest value the signal has ever had. For a waveguide length of 30 m, a simulated time of 100 ns is appropriate. Using a shorter waveguide or simulation time may compromise the results, e.g. due to a remaining ripple of the signal. It is recommended to excite the waveguide with a hard source.

8.2.1.8 Dielectric parameters

The waveguide shall be simulated with three homogeneous isotropic materials:

ε_r = 1,0; σ = 0,0 S/m

ε_r = 2,0: σ = 0,0 S/m

ε_r = 2,0; σ = 0,2 S/m

8.2.1.9 Signals to be recorded

The field components (E_Y for the TE mode and E_X or E_Z for the TM mode) shall be recorded at the locations specified in Figure 6 for the calculation of the numerical dispersion, as described below. For the TM mode, the components of the adjacent edges in the x- or z-directions can be chosen. The signals shall be extracted such that they directly correspond to the field values on the respective edges of the Yee-mesh. The use of interpolated data shall be avoided. The simulated signals in the time domain shall be extracted in the frequency domain. If the FDTD-code under evaluation is capable of transforming the time domain signals into the frequency domain, its built-in functions shall be used for the transformation. Otherwise, a DFT shall be applied to transform the signals. Zero padding shall not be used.

8.2.1.10 Calculation of the numerical dispersion

The numerical wave numbers $k_{x,\mathrm{num}}$ and $k_{z,\mathrm{num}}$ can be calculated from the Fourier-transformed fields recorded at the locations in Figure 6 using the identities

$$k_{x,\mathrm{num}} = -\frac{j}{\Delta s}\ln\frac{E_{01} + E_{21} - \sqrt{-4E_{11}{}^2 + (E_{01} + E_{21})^2}}{2E_{11}} \tag{19}$$

$$k_{z,\mathrm{num}} = -\frac{j}{\Delta s}\ln\frac{E_{10}+E_{12}-\sqrt{-4E_{11}{}^2+(E_{10}+E_{12})^2}}{2E_{11}} \tag{20}$$

where

Δs is the distance between the locations of the recorded components (30 mm).

Only the principal value of the complex logarithms in Formulas (19) and (20) shall be evaluated, i.e. only the solution of the complex logarithm shall be regarded, whose imaginary part lies in the interval $(-\pi,\pi]$. The numerical wave number can be calculated using

$$k^2 = k_x^2 + k_z^2 \tag{21}$$

The reference solutions of the numerical wave vector in a homogeneous mesh for comparison with Formulas (19) and (20) can be obtained by solving the dispersion relation of the Yee-algorithm

$$\left(\frac{k\Delta s}{\omega\Delta t}\right)^2 \sin^2\frac{\omega\Delta t}{2} = \sin^2\frac{k_{x,\mathrm{num}}\Delta s}{2} + \sin^2\frac{k_{z,\mathrm{num}}\Delta s}{2} \tag{22}$$

Δs is the mesh step, Δt is the time step, and ω is the frequency. k is the physically correct wave number in the dielectric as given in Formula (23). $k_{x,\mathrm{num}}$ in the numerical model of the waveguide is identical to its physical counterpart k_x given below in Formula (24).The results for the inhomogeneous mesh shall be compared to the physical wave number Formula (23).

For comparison of the components of the numerical wave vector with their physical counterparts, the following expressions apply for lossless and lossy dielectrics:

$$k = \sqrt{\omega\mu_0(\omega\varepsilon_r\varepsilon_0 + j\sigma)} \tag{23}$$

$$k_x = \frac{\pi}{w} \tag{24}$$

$$k_z = \sqrt{k^2 - k_x^2} \tag{25}$$

8.2.1.11 Data reporting

The numerical wave numbers shall be evaluated as a function of the frequency. The numerical wave numbers shall be evaluated over the frequency range from 500 MHz to 2 GHz as stated above using a maximum frequency step of 1 MHz (see also Note 2 of Table 6). For homogeneous meshes, the maximum deviation of the real and the imaginary part (lossy materials only) from the theoretical numerical wave number shall be evaluated. For inhomogeneous meshes, the maximum deviation of the real and the imaginary part (lossy materials only) from the physical wave number shall be evaluated. Table 6 lists all quantities to be reported.

All results for Table 6 shall be evaluated and reported for the waveguides oriented along all three axes of the coordinate system, for two different orientations around its axis (rotate waveguide by 90°) and positive and negative propagation direction along the respective axis. In total, 12 versions of Table 6 are required. The time domain signals that are recorded during the simulation shall be transformed into the frequency domain, as described above. The maximum deviation of the numerical wave number obtained from the simulation from its reference value shall be reported. This maximum deviation is relevant for the compliance of the code.

Table 6 – Results of the evaluation of the numerical dispersion characteristics

	Limit for code compliance	TE			TM		
axis, direction of propagation and orientation							
ε_r		1	2	2	1	2	2
σ [S/m]		0	0	0,2	0	0	0,2
numerical f_{cutoff} [MHz]		1 247	882	n.a.	1 247	882	n.a.
maximum deviation of simulated $\mathrm{Re}\, k_z$ from numerical reference homogeneous mesh	± 2 %						
maximum deviation of simulated $\mathrm{Im}\, k_z$ from numerical reference homogeneous mesh	± 2 %	n.a.	n.a.		n.a.	n.a.	
maximum deviation of simulated $\mathrm{Re}\, k_x$ from numerical reference homogeneous mesh	± 2 %						
maximum deviation of simulated $\mathrm{Re}\, k_z$ from physical solution inhomogeneous mesh	± 10 %						
maximum deviation of simulated $\mathrm{Im}\, k_z$ from physical solution inhomogeneous mesh	± 10 %	n.a.	n.a.		n.a.	n.a.	
maximum deviation of simulated $\mathrm{Re}\, k_x$ from physical solution inhomogeneous mesh	± 10 %						

NOTE 1 The maximum deviation of the numerical evaluation shall be evaluated over the entire simulated frequency range (500 MHz to 2 GHz).

NOTE 2 The fequency range ± 5 % around the cut-off frequencies shall be excluded from the evaluation of the k_z components. This does not apply to the waveguide filled with the lossy dielectric.

NOTE 3 The cut-off frequencies have been determined for the numerical waveguide model considering the numerical dispersion error. Therefore, they deviate from their physical values.

8.2.2 Planar dielectric boundaries

8.2.2.1 General

The implementation of planar dielectric interfaces which are oriented along a mesh axis and coincide with a primary mesh line shall be tested using the waveguide configurations described in 8.2.1 (waveguide, excitation, meshes). They shall be evaluated using a homogeneous mesh with a resolution of 10 mm. A dielectric boundary shall be introduced at a distance of 120 mm or larger from the excitation. The dielectric boundary is oriented perpendicularly to the PEC walls and divides the waveguide into two regions. A permittivity $\varepsilon_r = \varepsilon_1 = 1$ shall be used for the region which contains the excitation. The permittivity of the other region shall be $\varepsilon_r = \varepsilon_2 = 4$. A lossless ($\sigma = 0$) dielectric (TE and TM) and a lossy dielectric (TE only) shall be simulated ($\sigma = 0{,}2$ S/m). The dielectric region extends to the end of the computational domain, and the length of the waveguide shall be chosen such that reflections from the mesh truncation of the computational domain do not reach the location at which the fields are recorded during the simulation.

For the evaluation of the numerical reflection coefficient at the dielectric boundary as a function of the frequency, the E-fields shall be extracted at positions analogous to those in Figure 6, from the excitation location and also from the dielectric interface inside the dielectric medium, i.e. the arrangement of the recording locations shown in Figure 6 shall be repeated in the region filled with the dielectric ε_2. Closed expressions for the numerical reflection coefficient for TE- and TM-waves according to [11] are

$$r_{\mathrm{TE}} = \frac{\sin(k_{1z}\Delta s) - \sin(k_{2z}\Delta s)}{\sin(k_{1z}\Delta s) + \sin(k_{2z}\Delta s)} \tag{26}$$

$$r_{\mathrm{TM}} = \frac{\varepsilon_1 \tan\frac{k_{2z}\Delta s}{2} - \varepsilon_2 \tan\frac{k_{1z}\Delta s}{2}}{\varepsilon_1 \tan\frac{k_{2z}\Delta s}{2} + \varepsilon_2 \tan\frac{k_{1z}\Delta s}{2}} \tag{27}$$

Δs is the mesh step, and k_{1z} and k_{2z} are the numerical wave numbers in the two dielectrics, ε_1 and ε_2 and are required for the evaluation of r_{TE} and r_{TM}. They can be evaluated using Formula (20). For the evaluation of k_{2z} using Formula (20), the E-field components shall be recorded in the region filled with the dielectric ε_2, i.e. the recording locations as shown in Figure 6 shall be shifted by +120 mm along the z-axis.

Enhanced methods or special techniques, which deviate from the formulation of the Yee-algorithm as defined in Clause 5, shall be validated if they are used for the evaluation of particular testing configurations. Special techniques are permitted if they reduce the deviation from the physically correct with respect to the the numerical solution of Formulas (26) and (27). The applied method or technique has to be documented appropriately (e.g. by describing the definition of the update coefficients or modifications of the update equations). For the evaluation of the numerical reflection coefficient, the steps for the extraction of the numerical dispersion characteristics in free space as defined in 8.2.1 shall be repeated. The numerical reflection coefficient shall then be evaluated according to 8.2.2.2.

8.2.2.2 Extraction of the reflection coefficient

The amplitudes of the propagating and the reflected waves E_{p} and E_{r} are

$$E_{\mathrm{p}} = \left[E_{10}e^{-jk_z(2z_{\mathrm{r}} - z_0 - z_{11})} - E_{11}e^{-jk_z(2z_{\mathrm{r}} - z_0 - z_{10})}\right] / \Psi \tag{28}$$

$$E_{\mathrm{r}} = \left[E_{11}e^{-jk_z(z_{10} - z_0)} - E_{10}e^{-jk_z(z_{11} - z_0)}\right] / \Psi \tag{29}$$

where

$$\Psi = e^{-jk_z[2(z_{\mathrm{r}} - z_0) + z_{10} - z_{11}]} - e^{-jk_z[2(z_{\mathrm{r}} - z_0) + z_{11} - z_{10}]} \tag{30}$$

Here, z_{r} and z_0 are the locations of the boundary and the source, respectively. z_{10} and z_{11} are the positions of the E-field sensors as shown in Figure 6. k_x, k_{1z} and k_{2z} are the components of the numerical wave vector evaluated with Formulas (19) and (20). The amplitude reflection coefficient r is then calculated as

$$r = \frac{E_{\mathrm{r}}}{E_{\mathrm{p}}} \tag{31}$$

8.2.2.3 Data reporting

The numerical reflection coefficient r shall be evaluated as a function of the frequency, for reactive modes in a frequency range from 0,5 GHz to 0,6 GHz (below the cut-off frequency of the waveguides) and for propagating modes in a frequency range from 1,3 GHz to 2 GHz using a maximum frequency step of 1 MHz. For homogeneous meshes, the maximum deviation of the real and the imaginary part (lossy materials only) from the theoretical numerical wave number and reflection coefficient shall be evaluated. Table 7 lists all quantities to report.

All results for Table 7 shall be evaluated and reported for the waveguide oriented along all three axes of the coordinate system, for two different orientations around its axis (rotate waveguide by 90°) and positive and negative propagation direction along the respective axis. In total, 12 versions of Table 7 are required. The deviation of the simulated results from the numerical reference is relevant for the compliance of the code.

Table 7 – Results of the evaluation of the numerical reflection coefficient

	Limit for code compliance	**TE**		**TM**
axis, direction of propagation and orientation				
ε_r		4	4	4
σ [S/m]		0	0,2	0
maximum deviation of simulated $\mathrm{Re}\, k_{2z}$ from numerical reference 1,3 GHz < f < 2 GHz	± 5,0 %			
maximum deviation of simulated $\mathrm{Im}\{k_{2z}\}$ from numerical reference 0,5 GHz < f < 0,6 GHz	± 5,0 %	n.a.		n.a.
maximum deviation of simulated $\mathrm{Re}\, r$ from numerical reference 1,3 GHz < f < 2 GHz	± 5,0 %			
maximum deviation of simulated $\mathrm{Im}\, r$ from numerical reference 1,3 GHz < f < 2 GHz	± 5,0 %	n.a.		n.a.
maximum deviation of simulated $\mathrm{Re}\, r$ from numerical reference 0,5 GHz < f < 0,6 GHz	± 10,0 %			
maximum deviation of simulated $\mathrm{Im}\, r$ from numerical reference 0,5 GHz < f < 0,6 GHz	± 10,0 %	n.a.		n.a.
The frequency range is indicated for each value to be reported. NOTE Larger tolerances apply for the deviation of the simulation from the reference for frequencies between 0,5 GHz and 0,6 GHz (below cut-off).				

8.2.3 Absorbing boundary conditions

8.2.3.1 Aligned absorbing boundary conditions

The performance of an absorbing boundary condition (ABC) can be assessed analogously to the procedure used for the assessment of the numerical reflection at a dielectric boundary condition [29]. The computational domain (Figure 6) shall be filled homogeneously with vacuum (ε_r = 1, σ = 0) and truncated with an ABC at a position of z = 120 mm in front of the excitation. The reflection coefficient of the ABC can then be determined following the procedure described in 8.2.2, using a homogeneous mesh resolution of 10 mm and the inhomogeneous mesh for which coordinates are specified in 8.2.1, for a frequency range from 0,5 GHz to 3 GHz using a maximum frequency step of 1 MHz. In total, four simulations are required for each direction of propagation and for each orientation of the field vectors: TE with homogeneous mesh, TE with inhomogeneous mesh, TM with homogeneous mesh and TM with inhomogeneous mesh. Figure 7 indicates the limits for the maximum permissible reflection coefficient as a function of the frequency. As outlined in 8.2.1, the broadband excitation is used to characterize the reflection coefficient as a function of the angle of incidence and for reactive waves. Figure 7 shows the limits (upper margin of the grey range) as a function of the frequency. For strongly inclined angles (low frequencies), the limits are relaxed, and no limit is specified for the reflection coefficient of reactive waves below 1 370 MHz (10 % above the numerical cut-off frequency of the waveguide). Since the impact of cutting off the reactive fields with absorbing boundary conditions strongly depends on the application, no general recommendations are made regarding their characteristics under these conditions.

NOTE Large deviations from the theoretical wave number within a limited or the entire frequency range may indicate a higher mode or spurious field components which are excited at the boundary. If this is the case, the evaluation of the reflection coefficient is not possible.

All results shall be evaluated and reported with respect to the range of the permissible power reflection coefficient indicated in Figure 7 for the 120 mm waveguide oriented along all three axes of the coordinate system, for TE and TM modes, for two different orientations around its axis (rotate waveguide by 90°) and positive and negative propagation direction along the respective axis. In total, 24 evaluations are required.

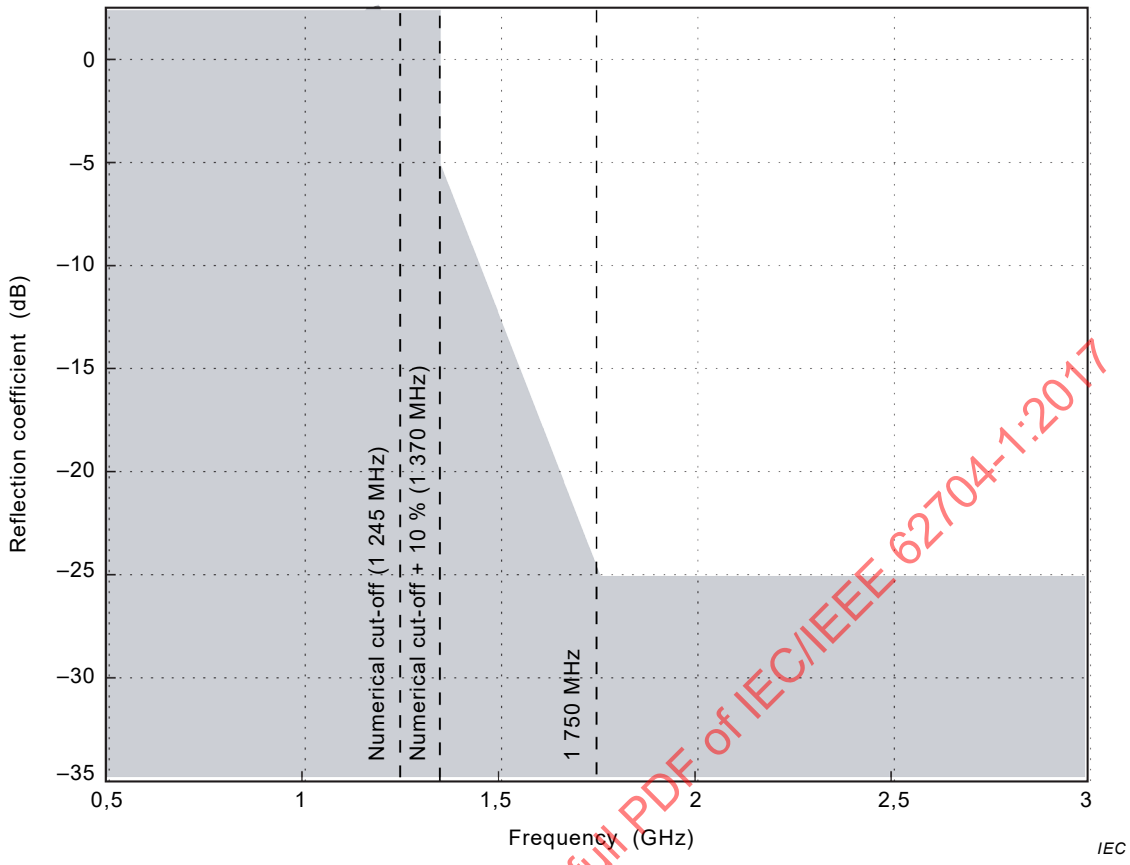

Figure 7 – Permissible power reflection coefficient (grey range) for the aligned absorbing boundary conditions

8.2.3.2 Performance of the ABCs in the corners of the computational domain

The numerical reflection of the absorbing boundary conditions in the corners of the computational domain shall be evaluated for tilting angle of 45° using the waveguide setup shown in Figure 8. Only a homogeneous mesh with a step size of 7 mm shall be evaluated. The width of the stair-cased waveguide can be assumed to be 118,8 mm = $12 \times 7 \times \sqrt{2}$ mm.

NOTE The effective numerical width of the stair-cased waveguide can be determined by evaluation of the numerical propagation constant.

Alternatively, a waveguide width of 120 mm can be used for more convenient modelling and meshing of the software under test. If a 120 mm waveguide is used, all dimensions and frequencies have to be scaled appropriately. Figure 8 shows the waveguide configuration and the positions of the E_y-field components to be recorded for the TE mode. The TE_1 mode can be excited by enforcing its analytical solution on the E_y components of the excitation. The TM_1 mode can be excited by enforcing its analytical solution on the E_x and E_z or its H_y components of the excitation. Alternative methods for the field excitation may be used, such as particular solvers to determine the propagating modes in the waveguide or preconfigured sources if the software provides them. It should be asserted that only the fundamental propagating mode exists at the location where the fields are recorded (Figure 8) because the presence of higher order modes or spurious modes will hinder the evaluation of the reflection coefficient.

Dimensions in millimetres

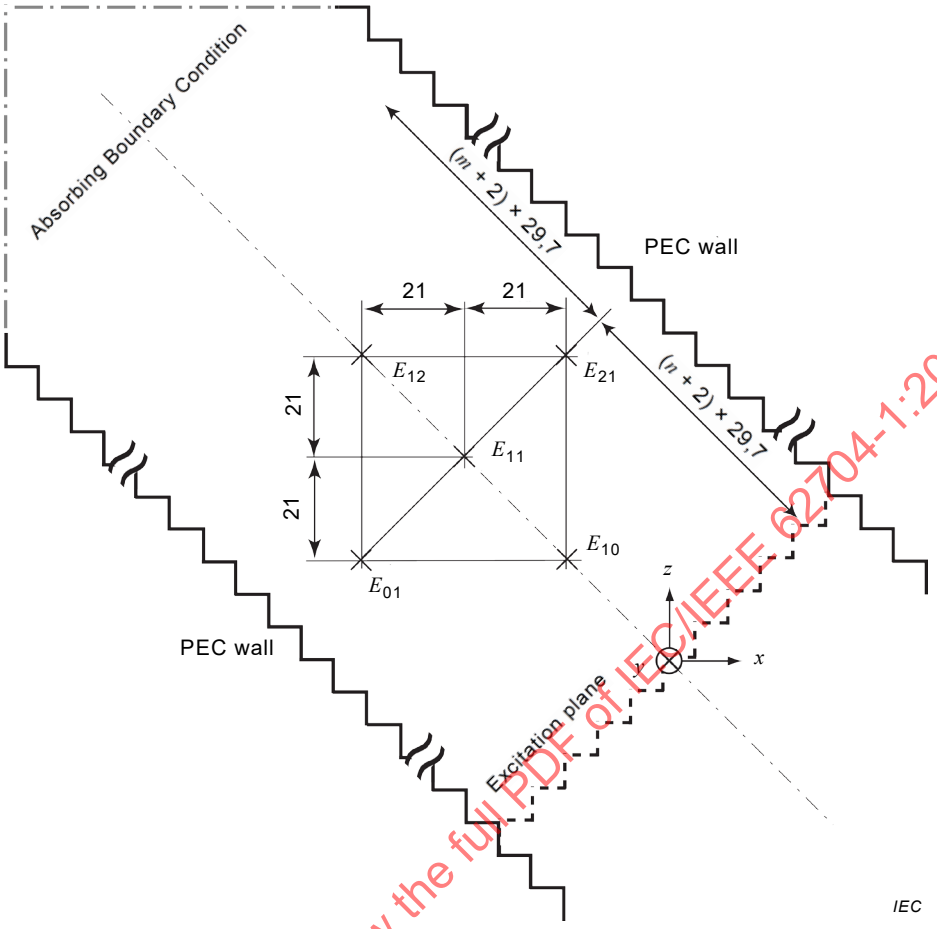

For TM-polarization, E_x, E_z or H_y-field components shifted by half a voxel are to be recorded (see text). The step size for the homogeneous mesh is 7 mm. The spacing between the source and the sensors is $(m + 2) \times 29{,}7$ mm = $(m + 2) \times 3 \times 7 \times \sqrt{2}$ mm. The spacing between the sensors and the boundary is $(n + 2) \times 29{,}7$ mm = $(n + 2) \times 3 \times 7 \times \sqrt{2}$ mm. m and n are arbitrary positive integers.

Figure 8 – Tilted parallel-plate waveguide terminated with absorbing boundary conditions and locations of the E_y-field components to be recorded for TE-polarization

For the assessment of the performance of the ABCs at the edges of the computational domain, the configuration described in Figure 8 shall be used to evaluate the reflection coefficient according to the procedure described in 8.2.2. For the numerical reflection coefficient in the edges of the computational domain, less restrictive conditions apply, i.e. the reflected power from the edges is allowed to be higher than the reflected power for the aligned case (Figure 7). For compliance of the code, the numerical reflection from the ABCs shall not exceed the limits indicated in the grey range of Figure 9. The reflection shall be evaluated and reported for all twelve edges of the computational domain for TE and TM mode. The reflection coefficients shall be reported as plots in graphs according to Figure 9. In total 24 plots are required.

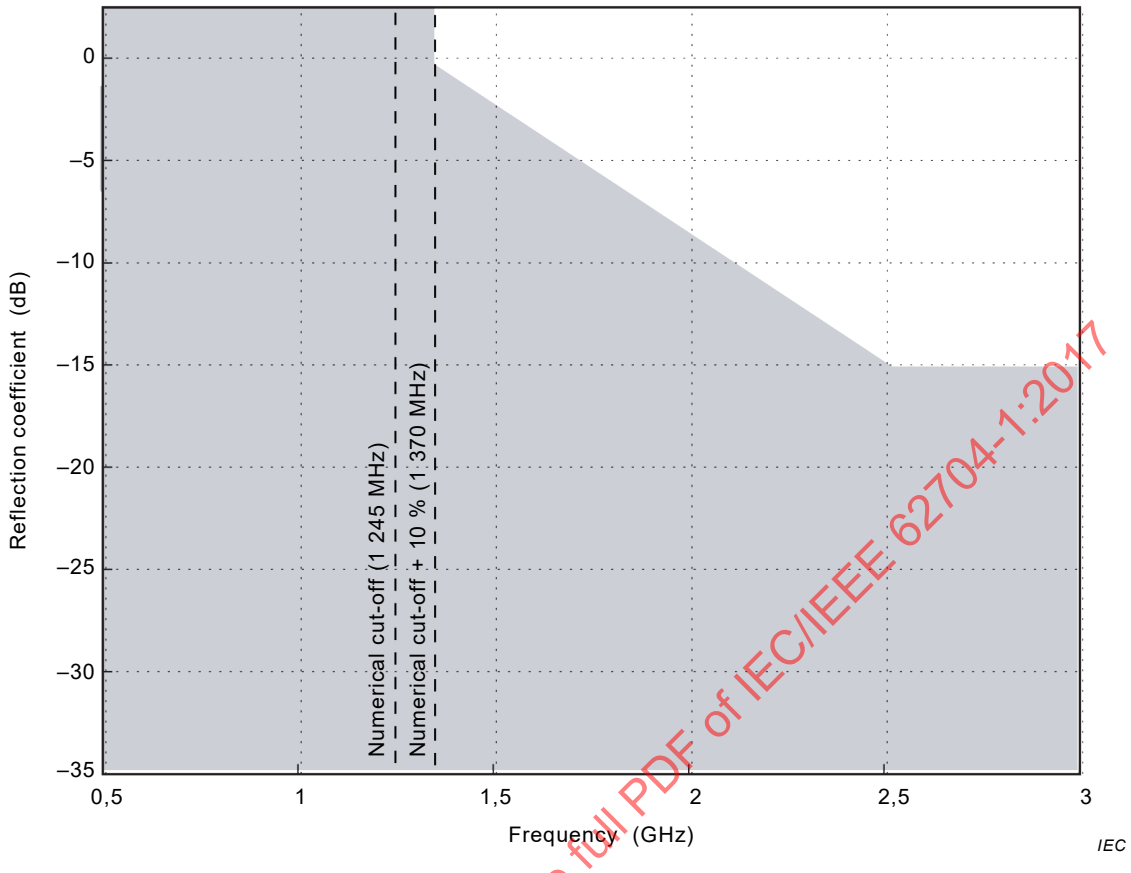

Figure 9 – Permissible power reflection coefficient (grey range) for the tilted absorbing boundary conditions

8.2.4 SAR averaging

Figure 10 and Figure 11 show the geometry for the testing of the averaging algorithm (SAR Star). The model consists of a cube with a cone on each face. The bottom of the cone is supported by a socket of reduced diameter. It consists of two different materials (core and shell) of different densities. The density of the core material and the embedded cube ($14 \times 14 \times 14$ mm^3 in the centre) is 2 000 kg/m^3, their relative permittivity is 12, and their conductivity is 0,15 S/m. The embedded cube is located in the centre of the SAR Star. It is surrounded by a 5 mm thick layer of background material. The density of the outer layer is 1 100 kg/m^3, its relative permittivity is 41, and its conductivity is 0,8 S/m. The embedded cube is separated from the outer two layers by a gap of 5 mm thickness. The gap consists of background material (white) and does not contribute to the averaging cube. The background material is lossless, its relative permittivity is 1, and its density is 0.

Dimensions in millimetres

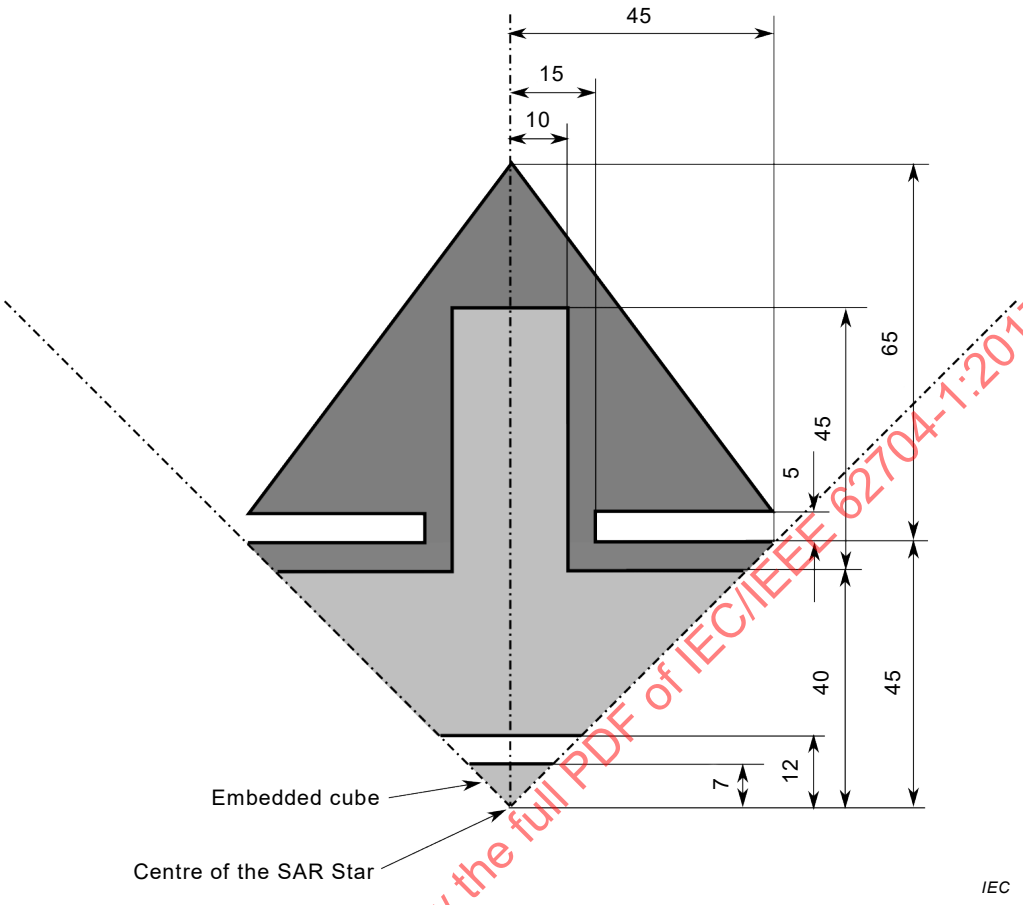

The core material and the embedded cube are light grey. The outer layer is dark grey. Background material and enclosed free space are white.

Figure 10 – Sketch of the testing geometry of the averaging algorithm

The structure covers all cases for the construction of the averaging volumes as described in 6.2 (used, unused and valid voxels) for all directions of space. It shall be meshed and voxelled in a homogeneous mesh ($\Delta x = \Delta y = \Delta z = 1$ mm) and an inhomogeneous mesh. The mesh coordinates are given in Annex B. The mesh lines correspond to the outline of the prevoxelled surfaces of the inhomogeneous SAR-Star model. When setting up the mesh, the user shall make sure that all surfaces are appropriately aligned with the mesh lines. Local and peak spatial-average SAR shall be calculated for an incident plane wave at a frequency of 900 MHz. The E-field vector of the plane wave shall be aligned to the x-axis, the H-field vector shall be aligned to the y-axis and the k-vector shall point along the positive z-axis of the SAR Star.

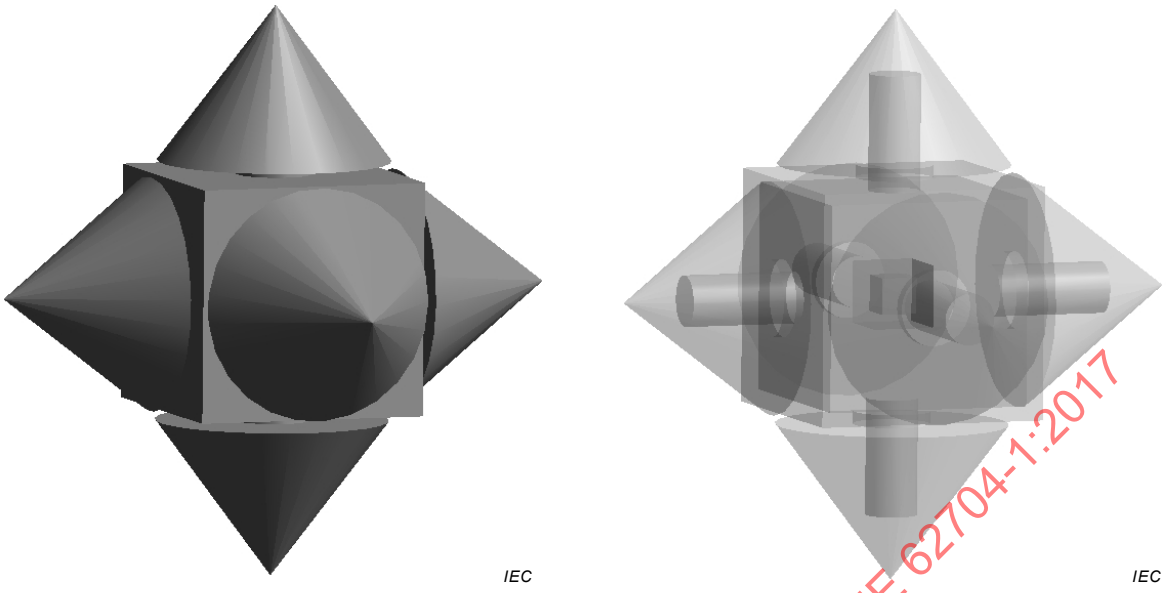

a) Outermost layer b) Transparent view

Figure 11 – 3D view of the SAR Star

The data to be reported for the compliance of the code are the status flags which have been assigned to each voxel (unused, used, valid), the orientation of expansion, the dimensions and the mass of the averaged cube which contains the target masses of 1 g and 10 g, the local voxel SAR and the peak spatial-average SAR assigned to each voxel. All status flags shall agree with the reference results, which are supplied online (B.3.2). The maximum deviations of the averaging mass and volume from the respective references is ±0,000 2 %. In case of averaging about a voxel located on the cube surface (6.2.2), these reference results contain more than one solution for those voxels for which more than one orientation of the averaging cube is allowed. For these voxels, the orientation that is reported by the software under evaluation shall agree with one of the orientations from the reference results and mass and volume shall be compared to the reference results with the same orientation. The maximum deviation of the spatial-average SAR value of the cube calculated by the software under evaluation lies within ±10 % of the maximum value of the multiple spatial average SAR values of all directions of expansion that are provided with the reference data results. The evaluation script for comparison with the reference results is given in B.3.3.

In order to test the averaging algorithm for deviation from the reference of no more than ±0,000 2 %, the averaging tolerance shall be set to ±0,000 1 % of the target mass. Depending on the software, this is either specified by the user or hardcoded in the implementation of the algorithm.

8.3 Canonical benchmarks

8.3.1 Generic dipole

The feed-point impedance of a $\lambda/2$-dipole (1 GHz) shall be evaluated for broadband excitation. If the software under test provides a harmonic simulation mode, the evaluation shall be carried out additionally in harmonic mode at 1 GHz. The dipole has a length of 150 mm and a diameter of 4 mm. The feeding gap size is 2 mm. The mesh shall be truncated with absorbing boundary conditions at 200 mm distance to the dipole in all directions. A broadband simulation covering the frequency range from 0,5 GHz to 1,5 GHz shall be performed. The radiated power shall be derived from the broadband simulation at 0,5 GHz, 1,0 GHz and 1,5 GHz. Reference results were derived with the method of moments. The homogeneous mesh has a step size of 2 mm. The minimum step of the inhomogeneous mesh is 1 mm (half of the feeding gap size) and the maximum step is 10 mm.

The quantities for evaluation and the maximum permitted error are given in Table 8. The power budget is defined as the deviation of the radiated power P_R from the feed-point power P_O (Clause C.5).

Table 8 – Results of the dipole evaluation

Quantity	Simulation result (Homogeneous mesh)	Simulation result (Inhomogeneous mesh)	Tolerance
Re Z at 1 GHz			40 Ω < Re Z < 140 Ω
Im Z at 1 GHz			30 Ω < Im Z < 130 Ω
Frequency for Im Z = 0			850 MHz < f < 950 MHz
Power budget at 0,5 GHz			< 5 %
Power budget at 1,0 GHz			< 5 %
Power budget at 1,50 GHz			< 5 %
NOTE The tolerances are the deviations which can be expected from a correctly implemented code which has passed the tests defined in 8.2. Larger deviations may indicate errors in the modeling or post-processing environment of the code under evaluation.			

8.3.2 Microstrip terminated with ABC

The propagation constant and wave impedance of a micro strip line and the reflection coefficient for quasi-TEM operation shall be evaluated. The micro strip has a characteristic impedance of 50 Ω. The substrate is lossless and has a relative permittivity of 3,4. The geometry of the strip line is given in Figure 12. For an impedance of 50 Ω, the width w of the strip line and the height h of the substrate shall be 2,8 mm and 1,2 mm, respectively.

The strip line shall be modelled in an inhomogeneous mesh with a minimum step size of 0,1 mm and a maximum step size of 1 mm. The thickness of the microstrip is negligible with respect to the other dimensions of the geometry. It can therefore be meshed as an infinitely thin sheet. Special techniques for the representation of thin sheets can be applied, but shall be validated according to 8.2, and their modifications to the update coefficients or the Yee-algorithm shall be documented. The microstrip shall be evaluated with its orientation aligned with the mesh. The strip line shall be terminated with ABCs. For the excitation, a broadband signal shall be used covering the frequency range from 0,5 GHz to 2,0 GHz. As a source, a single edge can be used or the quasi-TEM mode can be excited directly. The voltages and currents on the strip line shall be recorded at three points along the strip line in 30 mm distance from one another. The distance of the first of these points to the source shall be at least 30 mm (see location of the components E_{10}, E_{11} and E_{12} in Figure 6). The propagation constant and reflection coefficient shall be evaluated using the procedures described in 8.2.1 and 8.2.2. A sufficient distance between the source and the recording locations shall be kept in order to avoid the coupling of spurious components into the voltage and current sensors. When calculating the wave impedance, the phase offset between the voltage and current due to the leapfrog scheme shall be considered. The results to be reported are summarized in Table 9. For all quantities, the maximum error over the frequency range from 0,5 GHz to 2,0 GHz shall be reported.

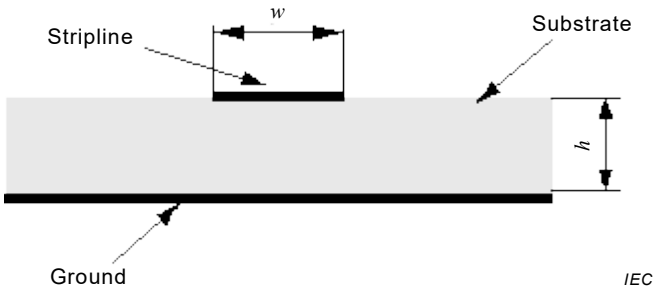

Figure 12 – Geometry of the microstrip line

Table 9 – Results of the microstrip evaluation

Quantity	Reference	Deviation	Tolerance
Re Z	50 Ω		45 Ω < Re Z < 55 Ω
Im Z	0		−2 Ω < Im Z < 2 Ω
Reflection coefficient	−∞ dB		< −20 dB

8.3.3 SAR calculation SAM phantom / generic phone

The benchmark described in Beard et al. [22] shall be repeated for the SAM phantom (D.3.1) with the generic phone in the “touch” and the “tilted” position (IEEE Std 1528) at 835 MHz and 1 900 MHz; 1 g and 10 g peak spatial-average SAR values shall be reported for the two positions and frequencies. The SAR results shall be normalized to the feed-point power, i.e. the accepted antenna power. They shall be within ±50 % of the mean values reported by Beard et al. [22] (Table 10), which corresponds to two times the reported standard deviation.

NOTE 1 The tolerance of ±50 % is approximately twice the largest standard deviations of the psSAR of the SAM phantom reported in [22]. A larger tolerance is permitted here because of the modifications of the SAR averaging algorithm described in 6.2.2.

NOTE 2 Supplemental information on the configuration can be found in Kainz et al. [30].

Table 10 – 1 g and 10 g psSAR for the SAM phantom exposed to the generic phone for 1 W accepted antenna power as specified in [22]

Quantity	835 MHz “touch”	835 MHz “tilted”	1 900 MHz “touch”	1 900 MHz “tilted”
1 g psSAR [W/kg]	7,5	4,9	8,3	12,0
10 g psSAR [W/kg]	5,3	3,4	4,8	6,8

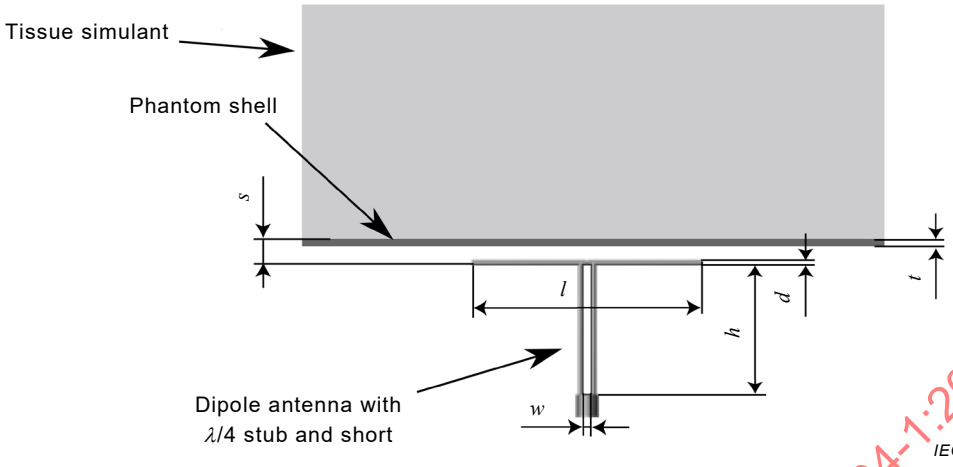

Figure 13 – Geometry of the setup for the system performance check according to [31]

8.3.4 Setup for system performance check

The dipole and flat phantom configuration for the system performance check defined in IEC 62209-1 and IEEE Std 1528 shall be simulated at 900 MHz and 3 000 MHz using the dielectric parameters given in Table 11 and the dimensions given in Table 12 and Figure 13. The height of the tissue simulant above the phantom shell shall be 150 mm. The parameters are:

f frequency of operation;

ε_r relative permittivity of the tissue simulant;

σ conductivity of the tissue simulant;

t thickness of the phantom shell;

d diameter of the rods of the dipole and of the $\lambda/4$ stub;

l length of the dipole;

h length of the $\lambda/4$ stub;

s distance from the bottom of the tissue simulant to the centre axis of the dipole rods;

w distance between the rods of the $\lambda/4$ stub;

x length of the phantom (along the dipole axis);

y width of the phantom;

z height of the tissue simulant.

The 1 g and the 10 g peak spatial-average SAR and the feed-point impedance shall be evaluated. The deviation of the peak spatial-average SAR and the real part of the feed-point impedance from the values reported in Table 13 shall not be larger than ±10 %. The imaginary part of the feed-point impedance shall be within ±5 Ω. Details on the numerical evaluation of the setup for the system performance check can be found in [31].

Table 11 – Dielectric parameters of the setup (Table 1 of [31])

f [MHz]	tissue simulant		phantom shell	
	ε_r	σ [S/m]	ε_r	σ [S/m]
900	41,5	0,97	3,7	0
3 000	38,5	2,4	3,7	0

Table 12 – Mechanical parameters of the setup (Tables 1 and 2 of [31])

f [MHz]	*t* [mm]	*d* [mm]	*l* [mm]	*h* [mm]	*s* [mm]	*w* [mm]	*x* [mm]	*y* [mm]	*z* [mm]
900	2,0	3,6	149,0	83,3	15,0	4,0	360,0	300,0	150,0
3 000	2,0	3,6	41,5	25,0	10,0	4,0	200,0	160,0	150,0

Table 13 – psSAR normalized to 1 W forward power and feedpoint impedance (Tables 3 and 4 of [31])

f [MHz]	1 g psSAR [W/kg]	10 g psSAR [W/kg]	Re *Z* [Ω]	Im *Z* [Ω]
900	11,0	7,07	49,9	2,3
3 000	65,4	25,3	53,4	–4,0

Annex A
(normative)

Fundamentals of the FDTD method

The original algorithm introduced by Yee in 1966 [5] forms the basis of the FDTD method where the electric and magnetic field components are positioned at the edges of a voxel and computed at alternate half time steps. Electromagnetic wave interactions in three-dimensions are solved with a system of six coupled partial differential equations. The resulting system of finite-difference equations requires only the adjacent field components from its previous time step to continue, and is highly adaptable to parallel processing.

The basic FDTD implementation is based on explicit, time staggered, and space staggered solution of discretized Maxwell's equations. For solutions in Cartesian coordinates, the field vectors $\mathbf{E}$ and $\mathbf{H}$ are dependent on the spatial variables x, y, z and the time variable t. The problem space is discretized into voxels $x = i\Delta x$, $y = j\Delta y$, $z = k\Delta z$, and time $t = n\Delta t$, where i, j and k are the voxel indices and n is the index of the time step. Using the central difference approximation for each field component, six explicit finite-difference equations are derived. Referring to [5], it can be noted that the electric field components are staggered half a mesh step with respect to the magnetic field components. For instance, the magnetic field component, H_z at time $(n + 1/2)$ is computed from the value H_z at time $(n - 1/2)$ and the values of the electric fields at time n along the voxel edges forming the contour in the plane normal to H_z, namely $E^n_{x_{i+1/2,j,k}}, E^n_{x_{i+1/2,j+1,k}}$, and $E^n_{y_{i,j+1/2,k}}, E^n_{y_{i+1,j+1/2,k}}$. Thus, Faraday's law is used to relate the line integral of the electric field to the normal flux component of the magnetic field in the mesh. Likewise, Ampere's law is used to update the electric fields. The staggered space-time stepping solution of the Maxwell's curl equations is known as the leapfrog algorithm. Figure A.1 shows the arrangement of the E- and H-field components. The algorithm consists of the so-called update equations for each electric field component and each magnetic field component. For the E_y- and the H_z-components, the update equations are written as

$$E^{n+1}_{y_{i,j+1/2,k}} = A_{y_{i,j,k}} E^n_{y_{i,j+1/2,k}} + B_{x_{i,j,k}} \left(H^{n+1/2}_{x_{i,j+1/2,k+1/2}} - H^{n+1/2}_{x_{i,j+1/2,k-1/2}} \right) - B_{z_{i,j,k}} \left(H^{n+1/2}_{z_{i+1/2,j+1/2,k}} - H^{n+1/2}_{z_{i-1/2,j+1/2,k}} \right) \quad \text{(A.1)}$$

$$H^{n+1/2}_{z_{i+1/2,j+1/2,k}} = H^{n-1/2}_{z_{i+1/2,j+1/2,k}} + C_{y_j} \left(E^n_{y_{i+1/2,j+1,k}} - E^n_{y_{i+1/2,j,k}} \right) - C_{x_i} \left(E^n_{x_{i+1,j+1/2,k}} - E^n_{x_{i,j+1/2,k}} \right) \quad \text{(A.2)}$$

The coefficients of these equations, the so-called update coefficients, are given as

$$A_{y_{i,j,k}} = \left(1 - \frac{\tilde{\sigma}_{y_{i,j,k}} \Delta t}{2\tilde{\varepsilon}_{y_{i,j,k}}} \right) \Bigg/ \left(1 + \frac{\tilde{\sigma}_{y_{i,j,k}} \Delta t}{2\tilde{\varepsilon}_{y_{i,j,k}}} \right) \quad \text{(A.3)}$$

$$B_{x_{i,j,k}} = \left(\frac{\Delta t}{\tilde{\varepsilon}_{y_{i,j,k}} \Delta z_k} \right) \Bigg/ \left(1 + \frac{\tilde{\sigma}_{y_{i,j,k}} \Delta t}{2\tilde{\varepsilon}_{y_{i,j,k}}} \right) \quad \text{(A.4)}$$

$$B_{z_{i,j,k}} = \left(\frac{\Delta t}{\tilde{\varepsilon}_{y_{i,j,k}} \Delta x_i} \right) \Bigg/ \left(1 + \frac{\tilde{\sigma}_{y_{i,j,k}} \Delta t}{2\tilde{\varepsilon}_{y_{i,j,k}}} \right) \quad \text{(A.5)}$$

$$C_{x_i} = \frac{\Delta t}{\mu_0 \Delta y_j} \tag{A.6}$$

$$C_{y_i} = \frac{\Delta t}{\mu_0 \Delta x_i}\,. \tag{A.7}$$

It should be noted that this formulation includes no magnetic losses and the permeability of free space is μ_0 throughout the computational domain. Alternatively, the update coefficients can be derived based on the approach described in [32] as exponential time stepping.

$\tilde{\varepsilon}$ and $\tilde{\sigma}$ are the effective permittivity and conductivity of the mesh edges of the respective E-field components. They are calculated by averaging the dielectric properties of the surrounding voxels. Figure A.2 shows an E_y-component in the FDTD mesh surrounded by voxels with four different dielectrics. $\tilde{\varepsilon}$ and $\tilde{\sigma}$ for the update equation of this component are calculated as

$$\tilde{\varepsilon}_y = \frac{\varepsilon_1 \Delta x_1 \Delta z_2 + \varepsilon_2 \Delta x_2 \Delta z_2 + \varepsilon_3 \Delta x_1 \Delta z_1 + \varepsilon_4 \Delta x_2 \Delta z_1}{(\Delta x_1 + \Delta x_2)(\Delta z_1 + \Delta z_2)} \tag{A.8}$$

$$\tilde{\sigma}_y = \frac{\sigma_1 \Delta x_1 \Delta z_2 + \sigma_2 \Delta x_2 \Delta z_2 + \sigma_3 \Delta x_1 \Delta z_1 + \sigma_4 \Delta x_2 \Delta z_1}{(\Delta x_1 + \Delta x_2)(\Delta z_1 + \Delta z_2)}\,. \tag{A.9}$$

These definitions of $\tilde{\varepsilon}$ and $\tilde{\sigma}$ already consider variable mesh steps (see below). Expressions for the E_x- and E_z-components can be obtained by permuting the axis indices. The update coefficients of PEC edges shall be defined such that the electric field components on these edges are always kept at zero.

The time step for algorithm stability is given by the Courant condition or Courant, Friedrichs and Lewy (CFL) condition in Formula (A.10) [33]. For three-dimensional meshes with voxel edges of length Δx, Δy, Δz, and v as the maximum velocity of propagation in any medium in the problem, the time step size Δt is limited by

$$v\Delta t \leq \frac{1}{\sqrt{\frac{1}{(\Delta x)^2} + \frac{1}{(\Delta y)^2} + \frac{1}{(\Delta z)^2}}} \tag{A.10}$$

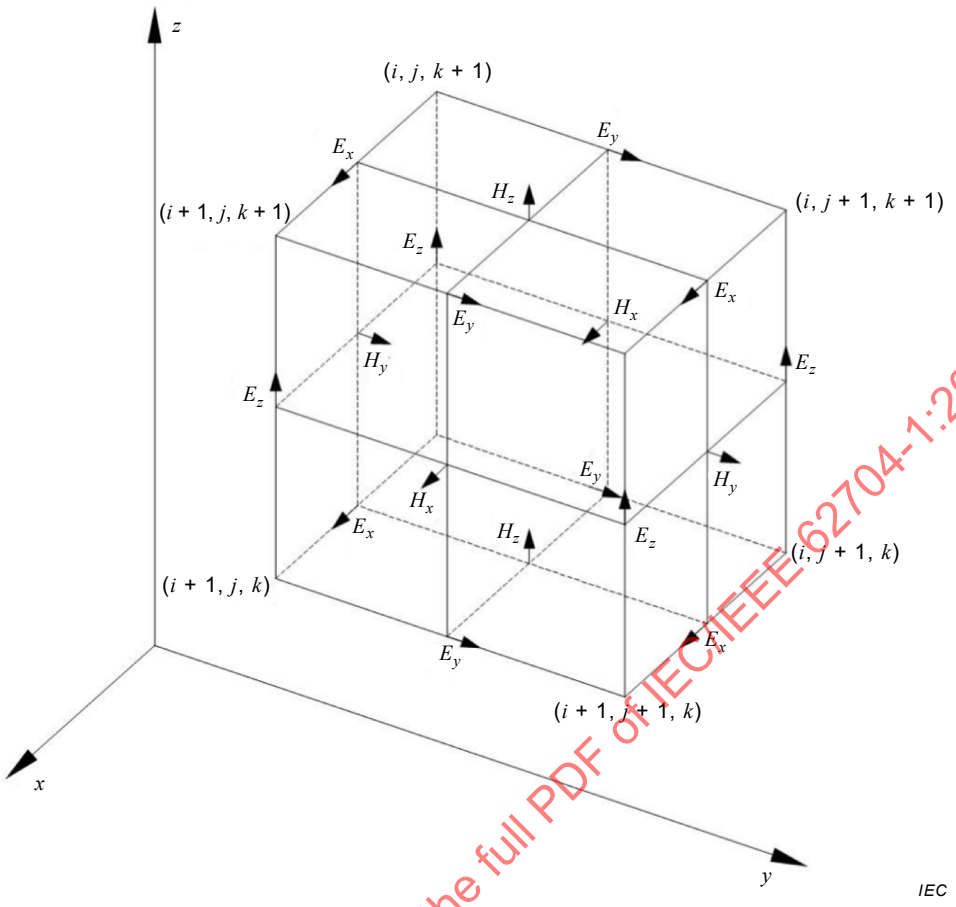

Figure A.1 – Voxel showing the arrangement of the E- and H-field vector components on a staggered mesh

For variable meshes where Δx, Δy, Δz are functions of x, y, and z, respectively, the maximum time step for stability is obtained from considering the voxel which produces the smallest time step.

The phase velocity of numerical modes in the FDTD lattice can vary with modal wavelength, direction of propagation, and lattice discretization, causing dispersion of the simulated wave modes in the computational domain. This numerical dispersion can lead to nonphysical results such as pulse distortion, artificial anisotropy, and pseudo-refraction. The mesh size $(\Delta x, \Delta y, \Delta z)$ typically is selected such that for the highest frequency at which the solution is valid, maximum $(\Delta x, \Delta y, \Delta z) \leq 0{,}1\lambda$, where λ is the wavelength at that frequency in the most electrically dense penetrable material. This limits the numerical dispersion in most cases to an acceptable level. Under this condition, the error in the phase velocity of waves propagating in an arbitrary direction is not more than –1,3 %. Thus, in this case, a sinusoidal numerical wave traveling a distance of only 2λ develops a lagging phase error of about 9,4° (Taflove [8]). This error is linearly cumulative with the wave propagation distance. Often the FDTD voxels in at least part of the mesh are much smaller than $0{,}1\lambda$ in order to accurately describe small geometry features.

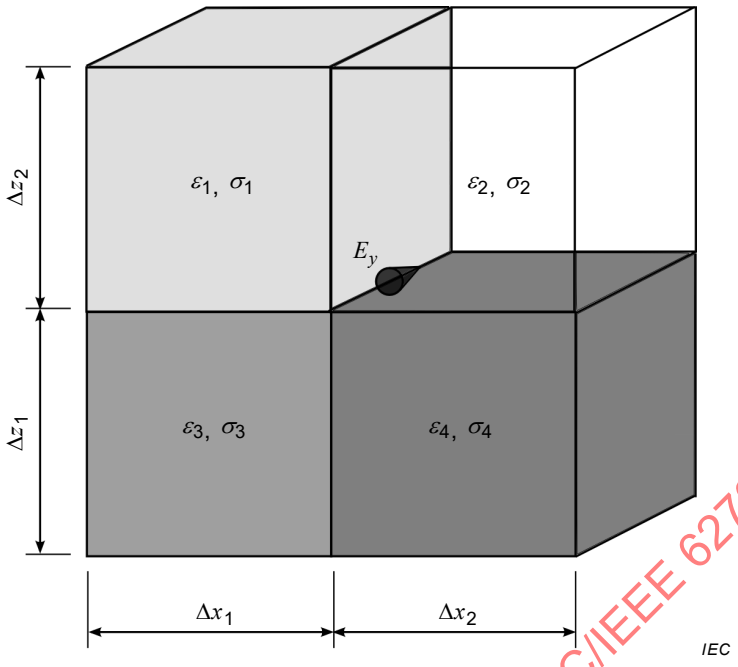

Figure A.2 – Voxels with different dielectric properties surrounding a mesh edge with an E_y-component

Annex B
(normative)

SAR Star

B.1 CAD files of the SAR Star

The geometry of the SAR Star is provided in two sets of STL-files. The STL-files contain discretized representations of the core material, the embedded cube and the outer layer of the SAR Star (8.2.4). Each of these solids is provided in a separate STL-file. The discretization of the solids follows the topology of the homogeneous mesh and the inhomogeneous mesh as given in B.2.2 and B.2.3. The code verification according to 8.2.4 shall be carried out using the discretized solids and the mesh lines in B.2.2 and B.2.3. All files can be downloaded from:

http://www.iec.ch/dyn/www/f?p=103:227:0::::FSP_ORG_ID,FSP_LANG_ID:1303,25.

B.2 Mesh lines for the SAR Star

B.2.1 General

The SAR Star benchmark (8.2.4) shall be carried out in a homogeneous and an inhomogeneous mesh. The mesh lines are given in B.2.2 for the homogeneous and in B.2.3 for the inhomogeneous topology. The geometrical centre of the SAR Star is located at the origin of the coordinate system set up by these mesh lines. The mesh contains additional space around the geometry of the SAR Star in order to yield a sufficiently large volume for the placement of the total field zone and for the reactive area of the scattered field.

B.2.2 Mesh lines for the homogeneous SAR Star

Mesh size (number of lines)

n_x 280
n_y 280
n_z 280

Mesh line coordinates [m] (x-, y- and z-axes):

−0,14; −0,139; −0,138; −0,137; −0,136; −0,135; −0,134; −0,133; −0,132; −0,131; −0,13; −0,129; −0,128; −0,127; −0,126; −0,125; −0,124; −0,123; −0,122; −0,121; −0,12; −0,119; −0,118; −0,117; −0,116; −0,115; −0,114; −0,113; −0,112; −0,111; −0,11; 0,109; −0,108; −0,107; −0,106; −0,105; −0,104; −0,103; −0,102; −0,101; −0,1; −0,099; −0,098; −0,097; −0,096; −0,095; −0,094; −0,093; −0,092; −0,091; −0,09; −0,089; −0,088; −0,087; −0,086; −0,085; −0,084; −0,083; −0,082; −0,081; −0,08; −0,079; −0,078; −0,077; −0,076; −0,075; −0,074; −0,073; −0,072; −0,071; −0,07; −0,069; −0,068; −0,067; −0,066; −0,065; −0,064; −0,063; −0,062; −0,061; −0,06; −0,059; −0,058; −0,057; −0,056; −0,055; −0,054; −0,053; −0,052; −0,051; −0,05; −0,049; −0,048; −0,047; −0,046; −0,045; −0,044; −0,043; −0,042; −0,041; −0,04; −0,039; −0,038; −0,037; −0,036; −0,035; −0,034; −0,033; −0,032; −0,031; −0,03; −0,029; −0,028; −0,027; −0,026; −0,025; −0,024; −0,023; −0,022; −0,021; −0,02; −0,019; −0,018; −0,017; −0,016; −0,015; −0,014; −0,013; −0,012; −0,011; −0,01; −0,009; −0,008; −0,007; −0,006; −0,005; −0,004; −0,003; −0,002; −0,001; 0,0; 0,001; 0,002; 0,003; 0,004; 0,005; 0,006; 0,007; 0,008; 0,009; 0,01; 0,011; 0,012; 0,013; 0,014; 0,015; 0,016; 0,017; 0,018; 0,019; 0,02; 0,021; 0,022; 0,023; 0,024; 0,025; 0,026; 0,027; 0,028; 0,029; 0,03; 0,031; 0,032; 0,033; 0,034; 0,035; 0,036; 0,037; 0,038; 0,039; 0,04; 0,041; 0,042; 0,043; 0,044; 0,045; 0,046; 0,047; 0,048; 0,049; 0,05; 0,051; 0,052; 0,053; 0,054; 0,055; 0,056; 0,057; 0,058; 0,059; 0,06; 0,061; 0,062; 0,063; 0,064; 0,065; 0,066; 0,067; 0,068; 0,069; 0,07; 0,071; 0,072; 0,073; 0,074; 0,075; 0,076; 0,077; 0,078; 0,079; 0,08; 0,081; 0,082; 0,083; 0,084; 0,085; 0,086; 0,087; 0,088; 0,089; 0,09; 0,091; 0,092; 0,093; 0,094; 0,095; 0,096; 0,097; 0,098; 0,099; 0,1; 0,101; 0,102; 0,103; 0,104; 0,105; 0,106; 0,107; 0,108; 0,109; 0,11; 0,111; 0,112; 0,113; 0,114; 0,115; 0,116; 0,117; 0,118; 0,119; 0,12; 0,121; 0,122; 0,123; 0,124; 0,125; 0,126; 0,127; 0,128; 0,129; 0,13; 0,131; 0,132; 0,133; 0,134; 0,135; 0,136; 0,137; 0,138; 0,139; 0,14;

B.2.3 Mesh lines for the inhomogeneous SAR Star

Mesh size (number of cells)
n_x 144
n_y 123
n_z 154

Mesh line coordinates [m]:

x-axis: −0,14; −0,139; −0,138; −0,137; −0,136; −0,135; −0,134; −0,133; −0,132; −0,131; −0,13; −0,129; −0,128; −0,127; −0,126; −0,125; −0,124; −0,123; −0,122; −0,121; −0,12; −0,119; −0,118; −0,117; −0,116; −0,115; −0,114; −0,113; −0,112; −0,111; −0,11; −0,109; −0,107; −0,106; −0,105; −0,104; −0,102; −0,100; −0,097; −0,092; −0,087; −0,083; −0,080; −0,077; −0,076; −0,075; −0,074; −0,073;−0,071; −0,068; −0,064; −0,059; −0,054; −0,049; −0,045; −0,04; −0,035; −0,03; −0,025; −0,022; −0,018; −0,015; −0,012; −0,01; −0,007; −0,003; 0,0; 0,003; 0,007; 0,009; 0,012; 0,015; 0,018; 0,022; 0,025; 0,028; 0,031; 0,033; 0,035; 0,037; 0,038; 0,039; 0,04; 0,041; 0,042; 0,043; 0,044; 0,045; 0,047; 0,049; 0,052; 0,057; 0,062; 0,067; 0,070; 0,072; 0,074; 0,075; 0,076; 0,077; 0,080; 0,083; 0,087; 0,092; 0,097; 0,100; 0,102; 0,104; 0,105; 0,106; 0,107; 0,109; 0,11; 0,111; 0,112; 0,113; 0,114; 0,115; 0,116; 0,117; 0,118; 0,119; 0,12; 0,121; 0,122; 0,123; 0,124; 0,125; 0,126; 0,127; 0,128; 0,129; 0,13; 0,131; 0,132; 0,133; 0,134; 0,135; 0,136; 0,137; 0,138; 0,139; 0,14;

y-axis: −0,14; −0,139; −0,138; −0,137; −0,136; −0,135; −0,134; −0,133; −0,132; −0,131; −0,13; −0,129; −0,128; −0,127; −0,126; −0,125; −0,124; −0,123; −0,122; −0,121; −0,12; −0,119; −0,118; −0,117; −0,116; −0,115; −0,114; −0,113; −0,112; −0,111; −0,11; −0,105; −0,1; −0,095; −0,09; −0,085; −0,08; −0,075; −0,071; −0,066; −0,062; −0,058; −0,054; −0,049; −0,045; −0,04; −0,035; −0,032; −0,028; −0,025;−0,022; −0,018; −0,015; −0,012; −0,01; −0,007; −0,003; 0,0; 0,003; 0,007; 0,009; 0,012; 0,015; 0,018; 0,022; 0,025; 0,028; 0,032; 0,035; 0,037; 0,04; 0,042; 0,045; 0,049; 0,054; 0,059; 0,064; 0,067; 0,071; 0,073; 0,075; 0,077; 0,079; 0,082; 0,084; 0,087; 0,09; 0,093; 0,096; 0,099; 0,102; 0,105; 0,109; 0,11; 0,111; 0,112; 0,113; 0,114; 0,115; 0,116; 0,117; 0,118; 0,119; 0,12; 0,121; 0,122; 0,123; 0,124; 0,125; 0,126; 0,127; 0,128; 0,129; 0,13; 0,131; 0,132; 0,133; 0,134; 0,135; 0,136; 0,137; 0,138; 0,139; 0,14;

z-axis: −0,14; −0,139; −0,138; −0,137; −0,136; −0,135; −0,134; −0,133; −0,132; −0,131; −0,13; −0,129; −0,128; −0,127; −0,126; −0,125; −0,124; −0,123; −0,122; −0,121; −0,12; −0,119; −0,118; −0,117; −0,116; −0,115; −0,114; −0,113; −0,112; −0,111; −0,11; −0,109; −0,107;−0,106;−0,105; −0,104; −0,103; −0,1; −0,097; −0,092; −0,087; −0,083; −0,08; −0,077; −0,076; −0,075; −0,074; −0,072; −0,070;−0,068; −0,064; −0,059; −0,054; −0,049; −0,045; −0,043; −0,04; −0,037; −0,035; −0,032; −0,029; −0,027; −0,026; −0,025; −0,024; −0,023; −0,022; −0,021; −0,02; −0,019; −0,018; −0,017; −0,016; −0,015; −0,013; −0,012; −0,010; −0,009; −0,007; −0,005; −0,003; −0,001; 0,0; 0,002; 0,004; 0,007; 0,01; 0,012; 0,014; 0,018;0,022; 0,025; 0,028; 0,032; 0,035; 0,037; 0,04; 0,042; 0,045; 0,049; 0,054; 0,059; 0,064; 0,068; 0,070; 0,072; 0,074; 0,075; 0,076; 0,077; 0,080; 0,083; 0,087; 0,092; 0,097; 0,1; 0,102; 0,104; 0,105; 0,106; 0,107; 0,108; 0,109; 0,11; 0,111; 0,112; 0,113; 0,114; 0,115; 0,116; 0,117; 0,118; 0,119; 0,12; 0,121; 0,122; 0,123; 0,124; 0,125; 0,126; 0,127; 0,128; 0,129; 0,13; 0,131; 0,132; 0,133; 0,134; 0,135; 0,136; 0,137; 0,138; 0,139; 0,14;

B.3 Evaluation of the SAR Star benchmark

B.3.1 General

For the evaluation of an implementation of the SAR averaging algorithm (6.2.2), the results of the SAR Star benchmark (8.2.4) shall be compared to reference results. These reference results are provided with this document for 1 g and 10 g averaging mass and for homogeneous and inhomogeneous meshes.

B.3.2 File format of the benchmark output

The output file for validation is a text file with rows for each voxel for which a spatial-average SAR value is calculated. Each row has nine tab-delimited entries (floating point or integer numbers as ASCII – American Standard Code for Information Interchange – or Unicode text) separated by white space. Separate files for the 1 g and the 10 g psSAR shall be provided. The line format is:

```
i j k status mass volume orientation local_SAR avg_SAR
```

with

– `i,j,k` mesh indices to the voxel location corresponding to the x-, y- and z-axes
– `status` flags (UNUSED=1, USED=2, VALID=3)
– `mass` averaging mass assigned to the voxel [g]
– `volume` averaging volume assigned to the voxel [mm^3]
– `orientation` orientation of the averaging cubes with respect to the reference location:

  face-centred cube $-x$ (=1), $+x$ (=2), $-y$ (=3), $+y$ (=4), $-z$ (=5) and $+z$ (=6), volume centred cube (=7)
– `local_SAR` unaveraged SAR assigned to the voxel [W/kg]
– `avg_SAR` 1 g or 10 g spatial-average SAR assigned to the voxel [W/kg]

The file shall only contain lines with voxels to which a psSAR value is assigned. The voxel data shall be sorted by their indices `i,j,k` starting with the smallest value and the index `k` increasing the fastest.

The benchmark output shall be compared to reference results using the script provided in B.3.3. The script is written in a high-level programming language, primarily intended for numerical computations. An open source implementation of this language is available. The paths to the files with the results to be validated and with the reference results have to be specified at the beginning of the script. The script will report if the validation is successful or will show where differences were found. All files can be downloaded from: http://www.iec.ch/dyn/www/f?p=103:227:0::::FSP_ORG_ID,FSP_LANG_ID:1303,25.

B.3.3 Evaluation script

```
clear all

% Reference Result: replace this by the reference files for 1g or 10g and
% graded or uniform mesh
str_ref_file = 'sar_star_graded_ref_1g_2016_03_18';

% Result under test: replace this by the output file of your SAR algorithm
str_test_file = 'sar_result_under_test.txt';

% Log file for the test: replace the file name if needed
str_logFile = 'log_file.txt';

% maximum number of error messages to display per test
int_maxdisp = 10;


% Do not change anything below this line!

global id_logFile = fopen(str_logFile, 'w');

function LogOut(s)
    fprintf("%s\n", s);
    global id_LogFile;
    fprintf(id_LogFile, "%s\n", s);
end

function sarDest = ProcessReference(sarOrig, sarTest)
    n_lines = length(sarOrig);
    sarDest = zeros(length(sarTest), 9);
    %
    % Check for multiple entries with different
    % averaging directions. If a multiple entry
    % is found, its psSAR value is copied to the
    % previous line in a new column. The line
    % with the multiple entry is removed.
    %
    LogOut(sprintf('%d lines in reference, %d in test result', n_lines,
length(sarTest)));
    iAmbg = 0;
    sarDest(1,:) = sarOrig(1,:); % copy first line, then start loop with 2nd
```

```
    iOrig = 2;
    iDest = 2;

fprintf('...progress.....................................................100
%%\n');
    nProgress = int32(n_lines/80);
    while (iOrig <= n_lines)
        if (mod(iOrig,nProgress)==0)
            fprintf('#'); % print progress bar
        end

        % Test if the previous line has the same voxel
        % indices as the current one.
        if (sarOrig(iOrig, 1) == sarDest(iDest - 1, 1)) ...
            && (sarOrig(iOrig, 2) == sarDest(iDest - 1, 2)) ...
            && (sarOrig(iOrig, 3) == sarDest(iDest - 1, 3))

            % If the psSAR value of the current line is larger than
            % the one of the previous line, override the one of the
            % previous line.
            if sarOrig(iOrig, 9) > sarDest(iDest - 1, 9)
                sarDest(iDest - 1, 9) = sarOrig(iOrig, 9);
            end

            % if orientation is the same as in the test result
            if sarOrig(iOrig, 7)==sarTest(iDest - 1, 7)
                sarDest(iDest - 1, 7) = sarOrig(iOrig, 7); % copy orientation
                sarDest(iDest - 1, 6) = sarOrig(iOrig, 6); % also copy volume
                sarDest(iDest - 1, 5) = sarOrig(iOrig, 5); % and mass
            end

            % Make sure that the averaging status of both lines is
            % "Unused" (index = 1)
            if (abs(sarDest(iDest - 1, 4)) ~= 1) || (sarOrig(iOrig, 4) ~= 1)
                error(['Wrong averaging status for multiple entry in at indices ', ...
                    num2str(sarOrig(iOrig, 1)), ', ', num2str(sarOrig(iOrig, 2)), ...
                    ', ', num2str(sarOrig(iOrig, 3)), ' (i, j, k).'])
            end

            % mark that line as ambiguous by negative status flag
            sarDest(iDest - 1, 4) = -sarOrig(iOrig, 4);

            iOrig = iOrig + 1;
        else
            sarDest(iDest,:) = sarOrig(iOrig,:);
            iOrig = iOrig + 1;
            iDest = iDest + 1;
        end

    end
    fprintf('\n')
    LogOut(sprintf('%d lines in processed reference', iDest-1));
end
clc
more off
format long % high precision needed to see differences in volume and mass
disp('')
LogOut('IEC/IEEE 62704-1 SAR Star Evaluation Script')
LogOut('Version 1.1')
LogOut('July 31st, 2016')
disp('')
disp('Status, mass and volume are tested for all voxels. The spatial')
disp('average SAR is only tested for UNUSED voxels.')
disp('')
disp('Implemented and tested in GNU Octave version 4.00')
disp('')

list_str_quantities = {'Status', 'Mass', 'Volume', 'Spatial Average SAR'};
list_str_units = {'', 'g', 'mm^3', 'W/kg'};
list_int_columns = [4, 5, 6, 9];
list_flt_tolerances = [0, 2.e-6, 2.e-6, 0.2];
boo_alltestspassed = 1;
LogOut(['Loading "',str_test_file,'" ...']);
tabTest = load(str_test_file);
LogOut(['Loading "',str_ref_file,'" ...']);
tabOrig = load(str_ref_file);
tabRef = ProcessReference(tabOrig, tabTest);
if numel(tabTest) ~= numel(tabRef)
```

```
    error('The number of array elements in the input files does not agree.')
end
disp('')
disp('Beginning validation...')
disp('')

for i = 1:length(list_str_quantities)
    i_linesInTable = (1:length(tabRef));

    % The averaging mass and volume are not defined for 'used' voxels.
    % This is why their values are disregarded.
    if   strcmp(list_str_quantities{i},   'Mass')   ||   strcmp(list_str_quantities{i},
'Volume')
        i_linesInTable = find(tabRef(:, 4) ~= 2);

    % Test the spatial average SAR in ambiguous 'unused' voxels only.
    elseif strcmp(list_str_quantities{i}, 'Spatial Average SAR')
        i_linesInTable = find(tabRef(:, 4) == -1);
    end

    LogOut(sprintf("%s test (%d lines in table relevant):", ...
        list_str_quantities{i}, length(i_linesInTable)));
    if strcmp(list_str_quantities{i}, 'Status')
        % compare integer values (i. e., status)
        list_deviations = tabTest(i_linesInTable, list_int_columns(i)) - ...
                    abs(tabRef(i_linesInTable, list_int_columns(i)));
    else
        % compare floats with their list_flt_tolerances
        list_deviations = tabTest(i_linesInTable, list_int_columns(i)) ./ ...
                        tabRef(i_linesInTable, list_int_columns(i)) - 1;
    end

    % find and output maximum deviation if relevant
    [MaxErr, int_MaxErr] = max(abs(list_deviations));
    if int_MaxErr~=0
        if abs(list_deviations(int_MaxErr)) > 0.01*list_flt_tolerances(i)
            id = i_linesInTable(int_MaxErr);
            LogOut(sprintf('Maximum deviation at (i/j/k) %d %d %d:', ...
                tabTest(id,1), tabTest(id,2), tabTest(id,3)));
            LogOut(sprintf('    Reference: %.12g %s  Test: %.12g %s', ...
                tabRef(id, list_int_columns(i)), list_str_units{i}, ...
                tabTest(id, list_int_columns(i)), list_str_units{i}));
            if list_flt_tolerances(i) ~= 0
                LogOut(sprintf('  Deviation is %f%%, Tolerance is +/-%f%%.', ...
                    100 * list_deviations(int_MaxErr), ...
                    100 * list_flt_tolerances(i)));
            end
        end
    end

    if strcmp(list_str_quantities{i}, 'Spatial Average SAR')
        list_int_errors = find(list_deviations < -list_flt_tolerances(i));
    else
        list_int_errors = find(abs(list_deviations) > list_flt_tolerances(i));
    end

    int_nErrors = length(list_int_errors);
    LogOut(sprintf('%d Deviations >%f percent', int_nErrors, list_flt_tolerances(i)));
    for ierr = 1:min(int_nErrors, int_maxdisp)
        id = i_linesInTable(list_int_errors(ierr));
        LogOut(sprintf('Error at (i/j/k) %d %d %d:', ...
            tabTest(id,1), tabTest(id,2), tabTest(id,3)));
        LogOut(sprintf('    Reference: %.12g %s  Test: %.12g %s', ...
            tabRef(id, list_int_columns(i)), list_str_units{i}, ...
            tabTest(id, list_int_columns(i)), list_str_units{i}));
              if list_flt_tolerances(i) ~= 0
            LogOut(sprintf('    Deviation is %f%%, Tolerance is +/-%f%%.', ...
                100 * list_deviations(list_int_errors(ierr)), ...
                100 * list_flt_tolerances(i)));
        end
    end

    if int_nErrors == 0
        LogOut('*** PASSED ***')
    else
        boo_alltestspassed = 0;
        if int_nErrors - int_maxdisp > 0
```

```
            LogOut(sprintf('           ...  and  %d  more  error(s).',  int_nErrors  -
int_maxdisp));
        end
        LogOut('*** FAILED ***');
    end

    LogOut('');

end
if boo_alltestspassed == 1
    LogOut('*** ALL TESTS WERE PASSED. ***')
else
    LogOut('*** ONE OR MORE TESTS FAILED. ***')
end
fclose(id_LogFile);
```

Annex C
(informative)

Practical considerations for the application of FDTD

C.1 Overview

The FDTD method was introduced to electromagnetic computations by Yee [5]. It was first used to evaluate absorption in heterogeneous tissues in 1975 (Taflove and Brodwin [4]) and it was not until late 1980s to early 1990s that FDTD was used to solve a broad range of electromagnetic problems. A brief history of major developments in FDTD can be found in a book by Taflove [8]. Comprehensive treatments of the method and its applications are given in books by Kunz and Luebbers [7] and Taflove [8].

The use of FDTD for evaluation of SAR in tissues has been described for a number of applications. Simple models used to simulate the tissue, such as cylinders (Umashankar and Taflove [34]; Furse et al. [35]; Taflove and Brodwin [36]; Borup et al. [37]) and spheres (Holland et al. [27]; Gao and Gandhi [38]), have been used to model exposure to plane waves. The SAR distributions in more realistic models of the human body exposed to plane waves (Sullivan et al. [39]; Chen and Gandhi [40]; Gandhi et al. [41]; Dimbylow and Gandhi [42]; Bernardi et al. [43]), or local sources (Gandhi et al. [44]; Tinniswood et al. [45], [46]; Bernardi et al. [47]), have also been investigated. Where comparisons with analytic solutions (for cylinders and spheres), or other methods or measurements have been made, the differences in the results were invariably well within the expected uncertainties.

In more recent years, numerous papers have been published on the SAR and performance of antennas on wireless devices placed in the vicinity of the human head. In many of these investigations MRI or CT derived high-resolution anatomical models of the human body were used. Antennas investigated range from monopole to various patches and diversity antennas. Representative studies are described in Dimbylow and Mann [48]; Jensen and Rahmat-Samii [49]; Gandhi et al. [50]; Watanabe et al. [51]; Okoniewski and Stuchly [52]; Toftgard et al. [53]; Hombach et al. [54]; Douglas et al. [55]; Pisa et al. [56]; Beard et al. [22]; Kainz et al. [30].

The FDTD method (Yee [5]; Kunz and Luebbers [7]; Taflove [8]) is a numerical algorithm for solving Maxwell's differential equations of electromagnetic field interactions in the time domain. The problem space is discretized into voxels where the space and time derivatives of the electric and magnetic fields are directly approximated by simple, second-order accurate central-difference equations. Computations of the electric and magnetic field components are interleaved in both space and time to permit tangential field continuity at media interfaces through a system of equations that are fully explicit. This allows for implementation of simple, direct algorithms with reduced computer storage, where the execution time is proportional to the electrical size of the problem space. Absorbing boundary conditions are used to terminate the computational domain to facilitate wave propagation into infinite free space. Phenomena such as electromagnetic scattering, aperture penetration, cavity excitation or wave interactions with biological tissues can be modelled in the FDTD space lattice comprised of voxels where electrical permittivity and conductivity are assigned to the electric field components of the lattice voxels. For far field exposure, an incident plane wave may be programmed to enter the computation region. With realistic radiating structures such as wireless devices, the device can be modelled and excited with a sinusoidal or pulse signal during the time-stepping process. The algorithm is time-stepped until the desired late-time pulse response or steady-state behaviour is observed.

With cubical or rectangular voxels, the electric field vector component is surrounded by four circulating magnetic field vector components, and vice versa. This arrangement of field components also permits implementation of the integral form of Faraday's law and Ampere's law at the voxel level, allowing physically thin slots and wires or curved surfaces to be incorporated into existing FDTD algorithms. FDTD solutions for three-dimensional complex biological geometries at millimetre resolutions have been used to study SAR distributions associated with wireless devices (Gandhi et al. [44]; Gandhi and Chen [57]; Jensen and Rahmat-Samii [49]; Dimbylow and Mann [48]; Luebbers et al. [58]; Beard et al. [22]; Kainz et al. [30]). More details on the FDTD method for evaluating SAR from wireless communications devices can be found in Clauses C.2 to C.6.

C.2 Practical considerations

C.2.1 Computational requirements

The time variation of the excitation may be either pulsed or sinusoidal. The advantage of using a pulsed excitation is that the response for a wide frequency range can be obtained. For accurate results, however, the frequency dependent behaviour of the biological materials should be included in the calculations. Methods for doing this are well known (Kunz and Luebbers [7]; Taflove [8]) so that transient electromagnetic field amplitudes for pulse excitation can be calculated (Gandhi et al. [41]; Furse et al. [59]). Sine wave excitation is preferred when results at only a single frequency or at a few frequencies are desired. This is especially convenient if results for the entire body are needed, such as the SAR distribution, since storing the transient results for the entire body mesh and applying Fast Fourier Transformation (FFT) to calculate the SAR versus frequency requires extremely large amounts of computer storage. An alternative to applying the FFT is to apply a running Discrete Fourier Transformation (DFT) which is evaluated for a few specific frequencies. This provides a reasonably efficient approach when results at a few frequencies are needed rather than the entire spectrum.

The choice of voxel size is critical in applying FDTD. It should be small enough to provide accurate results at the highest frequency of interest, and yet be large enough to keep resource requirements manageable. Voxel size is directly affected by the dielectric properties of the materials present. The greater the permittivity and/or conductivity the shorter the wavelength at a given frequency and the smaller the voxel size required. Once a voxel size is selected, the maximum time step is determined by the Courant stability condition. After the voxel size is determined, a problem space large enough to encompass the scattering object, plus space between the object and the outer absorbing boundary, is determined. From the number of voxels needed and the number of time steps required, resource requirements can be estimated (Formulas (C.1) and (C.2)).

Given the shortest wavelength of interest, the voxel dimensions are determined as one tenth of this wavelength (or less if greater accuracy is required). From this and the physical size of the problem geometry, the total number of voxels in the problem space can be determined. Assume that the material information for each voxel edge can be stored in 1 byte arrays with only indices of dielectric materials considered. An estimate of the computer storage required in bytes (assuming single-precision field variables) can be obtained from

$$M_s = 27 N_C \tag{C.1}$$

where

M_s are the memory requirements in bytes;

N_C is the total number of voxels in the problem space.

If magnetic materials are included, six edges are considered for the material arrays, and M_s increases to $30\,N_C$. The relatively small number of auxiliary variables needed for the computation process has been ignored since for a typical calculation nearly all of the required memory is used for the field variables. A simple estimation is that for each three million FDTD voxels approximately 100 megabytes of RAM will be required for the calculation.